

RESEARCH ARTICLE SUMMARY

VASCULAR BIOLOGY

Lysosomal dysfunction and inflammatory sterol metabolism in pulmonary arterial hypertension

Lloyd D. Harvey, Mona Alotaibi, Yi-Yin Tai, Ying Tang, Hee-Jung J. Kim, Neil J. Kelly, Wei Sun, Chen-Shan C. Woodcock, Sanya Arshad, Miranda K. Culley, Wadih El Khoury, Rong Xie, Yassmin Al Aaraj, Jingzi Zhao, Neha Hafeez, Rashmi J. Rao, Siyi Jiang, Vinny Negi, Anna Kirillova, Dror Perk, Annie M. Watson, Claudette M. St. Croix, Donna B. Stoltz, Ji Young Lee, Mary Hongying Cheng, Manling Zhang, Samuel Detmer, Edward Guzman, Rajith S. Manan, Rajan Saggar, Kathleen J. Haley, Aaron B. Waxman, Satoshi Okawa, Tae-Hwi Schwantes-An, Michael W. Pauciulo, Bing Wang, Amy Webb, Caroline Chauvet, Daniel G. Anderson, William C. Nichols, Ankit A. Desai, Robert Lafayatis, Mehdi Nouraei, Haodi Wu, Jeffrey G. McDonald, Susan Cheng, Ivet Bahar, Thomas Bertero, Raymond L. Benza, Mohit Jain, Stephen Y. Chan*

INTRODUCTION: Vascular inflammation regulates endothelial cell (EC) pathophenotypes, particularly in pulmonary arterial hypertension (PAH). Dysregulation of lysosomal activity and cholesterol metabolism causes inflammation, but their relevance to PAH is unclear.

RATIONALE: Lysosomal acidification depends on vacuolar H^+ adenosine triphosphatases (V-ATPases). Nuclear receptor coactivator 7 (NCOA7) binds to V-ATPases to control lysosomal function and is up-regulated in human ECs under proinflammatory stimuli and in PAH lung tissue. However, a mechanism that connects NCOA7 to vascular disease remains undefined.

RESULTS: In pulmonary arterial ECs and in PAH, cytokine induction of NCOA7 preserved lysosomal acidification and served as a homeostatic brake to constrain inflammation. Conversely, NCOA7 deficiency promoted lysosomal dysfunction and production of proinflammatory oxysterols and bile acids that immunoactivated ECs. Mice deficient for endothelial *Ncoa7* or exposed to the bile acid 7 α -hydroxy-3-oxo-4-cholestenoic acid displayed worsened EC immunoactivation and more severe PAH. In humans, an unbiased, metabolome-wide association study ($n = 2756$ PAH patients) identified a plasma signature of the same NCOA7-dependent oxysterols and bile acids that was

associated with PAH mortality ($P < 1.1 \times 10^{-6}$). Supporting a genetic predisposition to NCOA7 deficiency in genome-edited, inducible pluripotent stem cell-derived ECs, the intronic single-nucleotide polymorphism (SNP) rs11154337 in *NCOA7* regulated NCOA7 expression, lysosomal acidification, oxysterol and bile acid production, and EC immunoactivation. SNP rs11154337 was associated with PAH severity through 6-min walk distance and mortality in discovery [$n = 93$ patients, $P = 0.009$; hazard ratio (HR) = 0.54, 95% confidence interval (CI) (0.34–0.86)] and validation [$n = 630$ patients, $P = 2 \times 10^{-4}$; HR = 0.49, 95% CI (0.34–0.71)] cohorts. Using computational modeling of small-molecule binding to NCOA7, we synthesized an activator of NCOA7 that promoted lysosomal activity, abrogated oxysterol generation, prevented EC immunoactivation, and reversed rodent PAH.

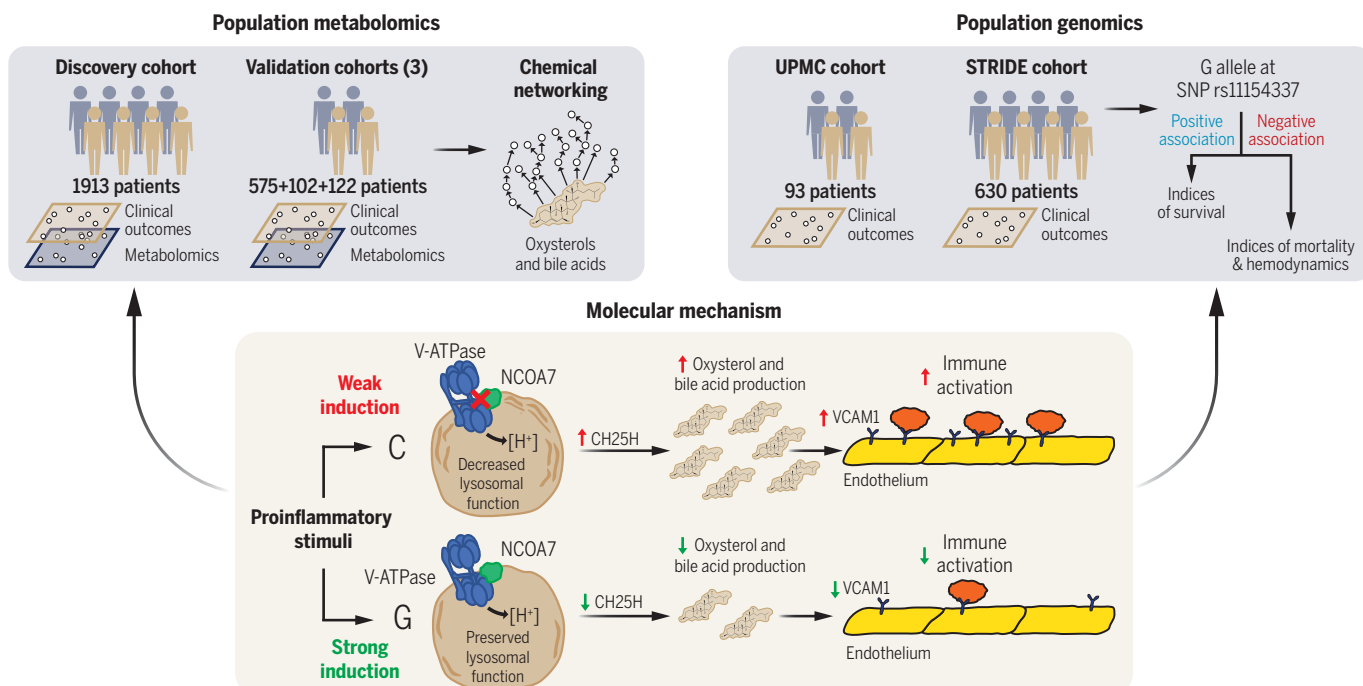
CONCLUSION: We established a genetic and metabolic paradigm that links lysosomal biology and oxysterol and bile acid processes to EC inflammation and PAH, thus carrying implications for diagnostic and therapeutic development. ■

The list of author affiliations is available in the full article online.

*Corresponding author. Email: chansy@pitt.edu

Cite this article as L. D. Harvey et al., *Science* **387**, eadn7277 (2025). DOI: 10.1126/science.adn7277

S READ THE FULL ARTICLE AT
<https://doi.org/10.1126/science.adn7277>



Multidimensional analyses of genomic and metabolomic datasets in combination with experimental validation define a SNP-dependent role for NCOA7 in lysosomal activity, oxysterol and bile acid production, endothelial immunoactivation, and the development of PAH. UPMC, University of Pittsburgh Medical Center; STRIDE, Sitaxsentan To Relieve Impaired Exercise; CH25H, cholesterol 25-hydroxylase; VCAM1, vascular cellular adhesion molecule 1.

RESEARCH ARTICLE

VASCULAR BIOLOGY

Lysosomal dysfunction and inflammatory sterol metabolism in pulmonary arterial hypertension

Lloyd D. Harvey^{1,2,3}, Mona Alotaibi^{4,5,6}, Yi-Yin Tai^{2,3}, Ying Tang^{2,3}, Hee-Jung J. Kim^{2,3}, Neil J. Kelly^{2,3,7}, Wei Sun^{2,3}, Chen-Shan C. Woodcock^{2,3}, Sanya Arshad^{2,3}, Miranda K. Culley^{1,2,3}, Wadih El Khoury^{2,3}, Rong Xie^{2,3}, Yassmin Al Aara^{2,3}, Jingxi Zhao^{2,3}, Neha Hafeez^{2,3}, Rashmi J. Rao^{2,3}, Siyi Jiang^{2,3}, Vinny Negi^{2,3}, Anna Kirillova^{2,3}, Dror Perk^{2,3}, Annie M. Watson^{2,3}, Claudette M. St. Croix⁸, Donna B. Stoltz⁸, Ji Young Lee^{9,10}, Mary Hongying Cheng^{9,10}, Manling Zhang^{2,3,7}, Samuel Detmer¹¹, Edward Guzman^{12,13}, Rajith S. Manan¹⁴, Rajan Saggar^{15,16}, Kathleen J. Haley¹⁷, Aaron B. Waxman¹⁷, Satoshi Okawa^{2,3,18,19}, Tae-Hwi Schwantes-Arn^{20,21}, Michael W. Pauciulo²², Bing Wang^{2,3}, Amy Webb²³, Caroline Chauvet²⁴, Daniel G. Anderson¹², William C. Nichols²², Ankit A. Desai²¹, Robert Lafyatis²⁵, S. Mehdi Nouraie²⁶, Haodi Wu^{2,3}, Jeffrey G. McDonald^{27,28}, Susan Cheng²⁹, Ivet Bahar^{9,10}, Thomas Bertero²⁴, Raymond L. Benza³⁰, Mohit Jain^{5,6}, Stephen Y. Chan^{2,3*}

Vascular inflammation regulates endothelial pathophenotypes, particularly in pulmonary arterial hypertension (PAH). Dysregulated lysosomal activity and cholesterol metabolism activate pathogenic inflammation, but their relevance to PAH is unclear. Nuclear receptor coactivator 7 (NCOA7) deficiency in endothelium produced an oxysterol and bile acid signature through lysosomal dysregulation, promoting endothelial pathophenotypes. This oxysterol signature overlapped with a plasma metabolite signature associated with human PAH mortality. Mice deficient for endothelial *Ncoa7* or exposed to an inflammatory bile acid developed worsened PAH. Genetic predisposition to NCOA7 deficiency was driven by single-nucleotide polymorphism rs11154337, which alters endothelial immunoactivation and is associated with human PAH mortality. An NCOA7-activating agent reversed endothelial immunoactivation and rodent PAH. Thus, we established a genetic and metabolic paradigm that links lysosomal biology and oxysterol processes to endothelial inflammation and PAH.

Vascular inflammation regulates endothelial cell (EC) integrity and function across vascular disease states, including atherosclerosis (1), hypertension (2), stroke (3), and sepsis (4). Within the lung, endothelial inflammation is a feature of acute lung injury (5), pathogen-mediated processes (6), and pulmonary arterial hypertension (PAH). PAH is a deadly, enigmatic, and chronically progressive disease characterized by vessel remodeling and poorly defined molecular origins (7). Recent attention and debate have centered on EC inflammation as a causative factor, rather than a bystander, in controlling disease severity (8).

Molecular accelerators and brakes regulate homeostasis in EC inflammation (9), but the

specific levers are incompletely described. Dysfunctional lysosomal activity has been linked to inflammation (10). Central to the maintenance of lysosomal function is acidification of the luminal space, mediated by the vacuolar H⁺ adenosine triphosphatase (V-ATPase) family (11). Loss of this hydrolytic capacity leads to lysosomal storage disorders (LSDs), which can result in pulmonary vascular phenotypes (12–15). Nuclear receptor coactivator 7 (NCOA7) directly binds to and modulates V-ATPase activity (16–18) to control endolysosomal function and modulate pathogen entry (16, 19, 20), renal tubular acidification (21), and neuronal function (17). NCOA7 is up-regulated in human ECs by proinflammatory stimuli (22) and in PAH lung

tissue (23), but a causative mechanism that connects NCOA7 to cardiopulmonary vascular disease has not been defined.

Lysosomal dysfunction carries relevance to PAH (24). Downstream of acidification, lysosomes carry pH-sensitive, hydrolytic enzymes that break down cellular waste and direct macromolecular trafficking (25). Lysosomal activity is connected to autophagy and bone morphogenic protein receptor type 2 (BMPR2)-specific biology—processes that are relevant to PAH (26, 27). Loss of lysosomal hydrolase activity leads to accumulation of oxysterols and bile acids (28), bioactive molecules that are up-regulated in the plasma and lungs of PAH patients (29–31). Oxysterols and bile acids influence cholesterol biosynthesis and cell membrane properties, driving cellular defenses in adaptive and innate immunity (32). These molecules immunoactivate ECs (33), contributing to peripheral vascular diseases (34). As reported in our companion study (35), an unbiased plasma metabolomic analysis of 2756 PAH patients identified a metabolome-wide association (adjusted $P < 1.1 \times 10^{-6}$) of glucuronidated oxysterols and downstream bile acids with PAH disease severity and mortality. Given the connection of NCOA7 to lysosomal biology and an association of lysosome-derived oxysterol and bile acid levels with PAH, we sought to determine whether NCOA7 controls oxysterol and bile acid metabolism, pulmonary EC immunoactivation, and PAH—thus offering a mechanistic explanation for the metabolomic association with PAH severity (35).

Results

Convergent inflammatory regulation of NCOA7 across cellular, animal, and human instances of PAH

Given the association between lysosomal dysfunction and oxysterol and bile acid production (28), we sought to determine whether triggers of EC dysfunction and PAH control lysosomal behavior. To do so, we performed an unbiased, transcriptomic analysis on primary human pulmonary artery endothelial cells (PAECs) exposed to interleukin-1β (IL-1β) (1 ng/ml for 24 hours)—a proinflammatory cytokine elevated

¹Medical Scientist Training Program, University of Pittsburgh, Pittsburgh, PA, USA. ²Center for Pulmonary Vascular Biology and Medicine, Pittsburgh, Heart, Lung, and Blood Vascular Medicine Institute, University of Pittsburgh, Pittsburgh, PA, USA. ³Division of Cardiology, University of Pittsburgh School of Medicine, Pittsburgh, PA, USA. ⁴Division of Pulmonary and Critical Care Medicine, University of California San Diego, La Jolla, CA, USA. ⁵Department of Medicine, University of California, San Diego, La Jolla, CA, USA. ⁶Department of Pharmacology, University of California, San Diego, La Jolla, CA, USA. ⁷Division of Cardiology, Veterans Affairs Pittsburgh Healthcare System, Pittsburgh, PA, USA. ⁸Center for Biologic Imaging, University of Pittsburgh, Pittsburgh, PA, USA. ⁹Laufer Center for Physical and Quantitative Biology, Stony Brook University, Stony Brook, NY, USA. ¹⁰Department of Biochemistry and Cell Biology, Stony Brook University, Stony Brook, NY, USA. ¹¹Department of Chemistry, Massachusetts Institute of Technology, Boston, MA, USA. ¹²Institute of Medical Engineering and Science, Massachusetts Institute of Technology, Boston, MA, USA. ¹³School of Engineering and Applied Sciences, Harvard University, Cambridge, MA, USA. ¹⁴Department of Chemical Engineering, Massachusetts Institute of Technology, Boston, MA, USA. ¹⁵Department of Medicine, David Geffen School of Medicine, University of California, Los Angeles (UCLA), Los Angeles, CA, USA. ¹⁶Department of Pathology, David Geffen School of Medicine, UCLA, Los Angeles, CA, USA. ¹⁷Division of Pulmonary and Critical Care Medicine, Department of Medicine, Brigham and Women's Hospital, Harvard Medical School, Boston, MA, USA. ¹⁸Department of Computational and Systems Biology, University of Pittsburgh, Pittsburgh, PA, USA. ¹⁹McGowan Institute for Regenerative Medicine, University of Pittsburgh, Pittsburgh, PA, USA. ²⁰Department of Medical and Molecular Genetics, Indiana University, Indianapolis, IN, USA. ²¹Department of Medicine, Indiana University, Indianapolis, IN, USA. ²²Division of Human Genetics, Cincinnati Children's Hospital Medical Center, University of Cincinnati College of Medicine, Cincinnati, OH, USA. ²³Department of Biomedical Informatics, Ohio State University, Columbus, OH, USA. ²⁴Université Côte d'Azur CNRS, Institut de Pharmacologie Moléculaire et Cellulaire (IPMC), Sophia-Antipolis, Valbonne, France. ²⁵Division of Rheumatology and Clinical Immunology, University of Pittsburgh, Pittsburgh, PA, USA. ²⁶Division of Pulmonary, Allergy, and Critical Care Medicine, University of Pittsburgh, Pittsburgh, PA, USA. ²⁷Center for Human Nutrition, University of Texas Southwestern Medical Center, Dallas, TX, USA. ²⁸Department of Molecular Genetics, University of Texas Southwestern Medical Center, Dallas, TX, USA. ²⁹Department of Cardiology, Smidt Heart Institute, Cedars-Sinai Medical Center, Los Angeles, CA, USA. ³⁰Division of Cardiology, Icahn School of Medicine at Mount Sinai, New York, NY, USA.

*Corresponding author. Email: chansy@pitt.edu

in PAH plasma and known disease trigger (36). Lysosomal regulatory genes were up-regulated along with V-ATPase subunits, binding partners of NCOA7 that promote lysosomal acidification (Fig. 1A) (16–18). Correspondingly, IL-1 β up-regulated NCOA7—both the canonical, full-length isoform (NCOA7_{full}) and, to a greater extent, an alternative-start, short-length version of NCOA7 (NCOA7_{short}) at both transcript and protein levels (Fig. 1, B and C, and fig. S1, A to D). Specifically, exposure to the proinflammatory cytokine IL-6 and its soluble receptor (IL6Ra; 10 ng/ml for 24 hours), which has been linked to PAH

(36), preferentially induced the short-length isoform at the transcript level and both isoforms at the protein level (fig. S1, E to G). By contrast, hypoxia, a driver of PAH (7), only subtly induced the short-length protein isoform (fig. S1, G to I). These data indicate a potential role for the NCOA7 isoforms, particularly in proinflammatory PAH conditions.

In an inflammatory model of PAH, transgenic mice with constitutive pulmonary IL-6 expression demonstrated elevated *Ncoa7* expression in CD45 $^-$ /EpCAM $^-$ /CD31 $^+$ ECs isolated from lung tissue (fig. S1, J and K). This was also observed

in the pulmonary vessels of *Il6* transgenic mice (Fig. 1, D and E, and movies S1 and S2). Similarly, examining the *in situ* localization of NCOA7, there was marked and transmural up-regulation in pulmonary vessels with heightened expression predominantly localized to the endothelium and adventitia—in both the chronic hypoxia mouse model and the monocrotaline-exposed PAH rat model (fig. S1, L to O, and movies S3 and S4).

In human lung tissue from patients with Group I PAH, NCOA7 expression was elevated predominantly in endothelium and adventitial fibroblast

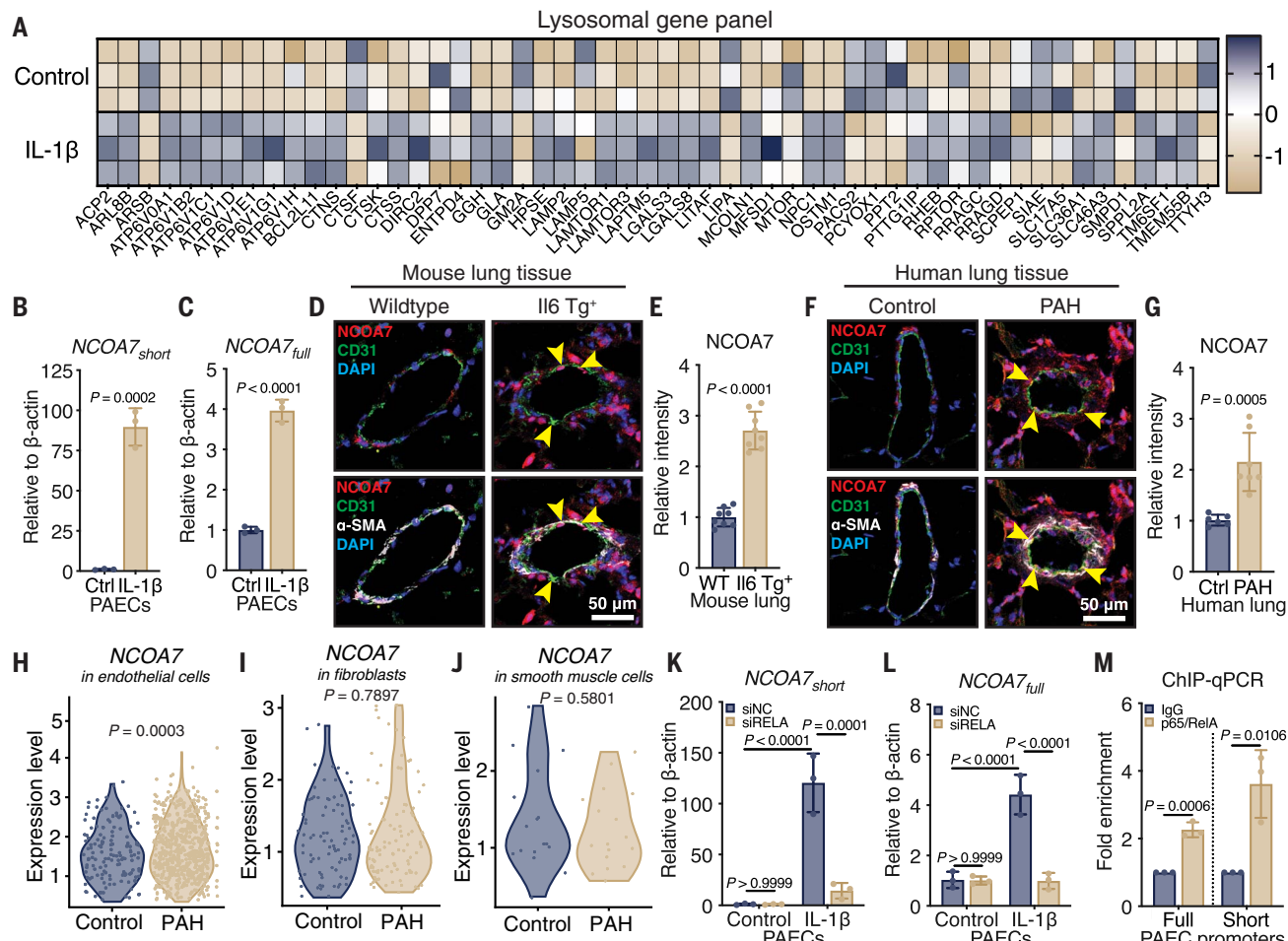


Fig. 1. Convergent inflammatory regulation of NCOA7 across cellular, animal, and human instances of PAH. (A) Transcriptomic analysis of human PAECs under control or IL-1 β ($n = 3$ replicates per group). Z-score is indicated as positive in blue and negative in gold. Genes listed have a false discovery rate (FDR)-corrected P value < 0.05 . (B) NCOA7_{short} expression by means of RT-qPCR ($n = 3$ replicates per group). (C) NCOA7_{full} expression by means of RT-qPCR ($n = 3$ replicates per group). (D) Immunofluorescent (IF) staining of NCOA7 (red with yellow arrowheads), CD31 $^+$ ECs (green), α -SMA $^+$ smooth muscle cells (white), and 4',6-diamidino-2-phenylindole (DAPI)-stained nuclei (blue) in pulmonary vessels of wild-type versus *Il6* Tg $^+$ mice. (E) Quantification of NCOA7 intensity in pulmonary vessels ($n = 8$ mice per group). (F) IF staining of NCOA7 (red with yellow arrowheads), CD31 $^+$ ECs (green), α -SMA $^+$ smooth muscle cells (white), and DAPI-stained nuclei (blue) in pulmonary vessels of healthy human controls versus PAH patients. (G) Quantification of NCOA7 intensity in pulmonary vessels ($n = 6$ to 7 patients per group). (H) NCOA7 expression in ECs identified by means of single-cell RNA-sequencing from lungs of healthy human controls or PAH patients ($n > 3$ patients per group). (I) NCOA7 expression in fibroblasts identified by means of single-cell RNA-sequencing from lungs of healthy human controls or PAH patients ($n > 3$ patients per group). (J) NCOA7 expression in smooth muscle cells identified by means of single-cell RNA-sequencing from lungs of healthy human controls or PAH patients ($n > 3$ patients per group). Cells were identified as expressing NCOA7 if the transformed expression value was > 0.2 . (K) NCOA7_{short} expression under RNA interference (RNAi) against *RELA* ($n = 3$ replicates per group). Two-way ANOVA. (L) NCOA7_{full} expression under RNAi against *RELA* ($n = 3$ replicates per group). Two-way ANOVA. (M) ChIP-qPCR against p65/RelA binding to full- and short-length promoter regions ($n = 3$ replicates per group). All data were analyzed by means of Student's *t* test unless otherwise specified and presented as mean \pm SD.

pulmonary vessels ($n = 6$ to 7 patients per group). (H) NCOA7 expression in ECs identified by means of single-cell RNA-sequencing from lungs of healthy human controls or PAH patients ($n > 3$ patients per group). (I) NCOA7 expression in fibroblasts identified by means of single-cell RNA-sequencing from lungs of healthy human controls or PAH patients ($n > 3$ patients per group). (J) NCOA7 expression in smooth muscle cells identified by means of single-cell RNA-sequencing from lungs of healthy human controls or PAH patients ($n > 3$ patients per group). Cells were identified as expressing NCOA7 if the transformed expression value was > 0.2 . (K) NCOA7_{short} expression under RNAi against *RELA* ($n = 3$ replicates per group). Two-way ANOVA. (L) NCOA7_{full} expression under RNAi against *RELA* ($n = 3$ replicates per group). Two-way ANOVA. (M) ChIP-qPCR against p65/RelA binding to full- and short-length promoter regions ($n = 3$ replicates per group). All data were analyzed by means of Student's *t* test unless otherwise specified and presented as mean \pm SD.

layers within pulmonary vessels when compared with healthy controls (Fig. 1, F and G, and movies S5 and S6). Yet by means of single-cell RNA-seqencing in lungs from idiopathic Group I PAH patients ($n = 3$) versus controls ($n = 5$) (23) of cells that expressed detectable NCOA7 levels, only endothelial—but not smooth muscle nor fibroblast—induction of NCOA7 was observed in PAH (Fig. 1, H to J). Patients were on standard-of-care pulmonary vasodilator medical therapy but not matched for exact regimens or PAH subtype. Yet the consistency of NCOA7 alterations across PAH samples suggested that vasodilators were not substantial confounders.

Thus, in proinflammatory models of PAH that used primary PAECs, rodent models, and human patients, we found that NCOA7 was up-regulated in the pulmonary vessel and, most consistently and robustly, the endothelium. However, because NCOA7 deficiency and consequent loss of lysosomal acidification should increase inflammation and worsen disease in other contexts (10), we hypothesized that NCOA7 acts as a homeostatic brake under proinflammatory stress to reduce disease through attenuation of EC immunoactivation.

To investigate upstream inflammatory mechanisms that modulate NCOA7, binding sites for the inflammatory transcription factor complex—the RelA/p65 (*RELA*) subunit of nuclear factor κ B (NF- κ B)—were predicted in the canonical (full-length) and noncanonical (short-length) NCOA7 promoter regions (37). Correspondingly, suppression of *RELA* in PAECs abrogated the IL-1 β -mediated up-regulation of both isoforms (Fig. 1, K and L). Chromatin immunoprecipitation with quantitative polymerase chain reaction (ChIP-qPCR) revealed an association of RelA/p65 at the canonical and noncanonical promoters (Fig. 1M), indicating promoter-transcription factor binding.

Loss of NCOA7 and mechanisms

Lysosomal dysfunction and lipid accumulation

To investigate a putative link between NCOA7 and oxysterol production in proinflammatory conditions, we characterized the NCOA7-mediated control of lysosomal acidification, given the function of lysosomes in sterol trafficking (38, 39). In human PAECs exposed to IL-1 β , NCOA7 suppression reversed the interleukin-specific alteration of the gene network that governs lysosomal function (Fig. 2A). A number of these genes encoded for subunits of V-ATPases—machinery necessary for lysosomal acidification.

Previous proteomics-based studies established that NCOA7 interacts with ATP6V1B1—a renal paralog of ATP6V1B2 (18, 40, 41). Correspondingly, in PAECs, NCOA7 abrogated IL-1 β -mediated up-regulation of ATP6V1B2, and the forced overexpression of short- or full-length isoforms up-regulated ATP6V1B2 (Fig. 2, B and C, and figs. S1, P to S, and S2A). In addition,

ATP6V1B2 was up-regulated in the pulmonary endothelium of rodent and human models of PAH (fig. S2, B to I). By means of proximity ligation assay, perinuclear staining consistent with lysosomal locations demonstrated specific ATP6V1B2-NCOA7 protein interactions (42). Moreover, lentiviral NCOA7_{short} or NCOA7_{full} overexpression up-regulated the number of ATP6V1B2-NCOA7 interactions in the lysosome (Fig. 2, D and E), which is consistent with the known function of the catalytic (TLDc) domain in both isoforms (43). These data demonstrated a role for both short- and full-length NCOA7 as regulatory components of the V-ATPase complex with putative downstream lysosomal function.

To assess NCOA7 activity in modulating lysosomal acidification, we used two measures of lysosomal enzyme activity. First, cleavage of the fluorescent Lysolive tracer (44) was increased by IL-1 β (or hypoxia) and subsequently blocked with loss of NCOA7 (Fig. 2, F and G, and fig. S2J). Second, lysosome-dependent cathepsin D activity assessed by means of SiR-Lysosome fluorescence (45) was up-regulated by IL-1 β and abrogated by NCOA7 deactivation (Fig. 2, H and I).

Reflecting lysosomal acidification, IL-1 β increased Lysosensor Green DND-189 fluorescent signal, which was reversed by NCOA7 suppression (Fig. 2J). Correspondingly, indicating enhanced lysosome luminal acidification, IL-1 β drove a shift to yellow fluorescence through the acidotropic probe Lysosensor Yellow/Blue DND-160 (46), a shift that was reversed by NCOA7 suppression (Fig. 2K). These observations correlated with findings in LSDs, in which undigested macromolecules accumulate in the lysosome (47). Loss of NCOA7 had no effect on other known lysosomal processes linked to PAH, namely autophagy or BMPR2 signaling (fig. S2, K to O).

Failure of V-ATPase complex formation or lysosomal acidification is a driver of lysosomal dysmorphology (48). Accordingly, morphologic analysis of lysosomes by use of transmission electron microscopy of human PAECs deficient for NCOA7 revealed marked hypertrophy of lysosomes (Fig. 2, L and M), denoting an inability to break down cellular components. The enlarged lysosomes in NCOA7-deficient cells carried lamellar-like inclusions (Fig. 2, L and M, yellow arrowheads), which is indicative of sterol buildup—phenocopying LSDs that present with abnormal sterol accumulation (28).

PAECs were costained by using a dye [boron-dipyromethene (BODIPY)] against neutral lipids and a dye (Lysotracker) that specifically localizes to acidic compartments. NCOA7 suppression increased lipid punctae within acidic vesicles, indicating lysosomal accumulation of lipids (Fig. 2, N and O). Yet in the context of intact NCOA7 induction and enhanced lysosomal acidification with IL-1 β , lipid content

was maintained, presumably reflecting the balance of other known aspects of IL-1 β -dependent cholesterol synthesis and homeostasis (49). These findings establish NCOA7 as a binding partner to the V-ATPase complex to promote lysosomal acidification and sterol processing in PAECs.

Reprogramming of sterol metabolism through abnormal lipid accumulation

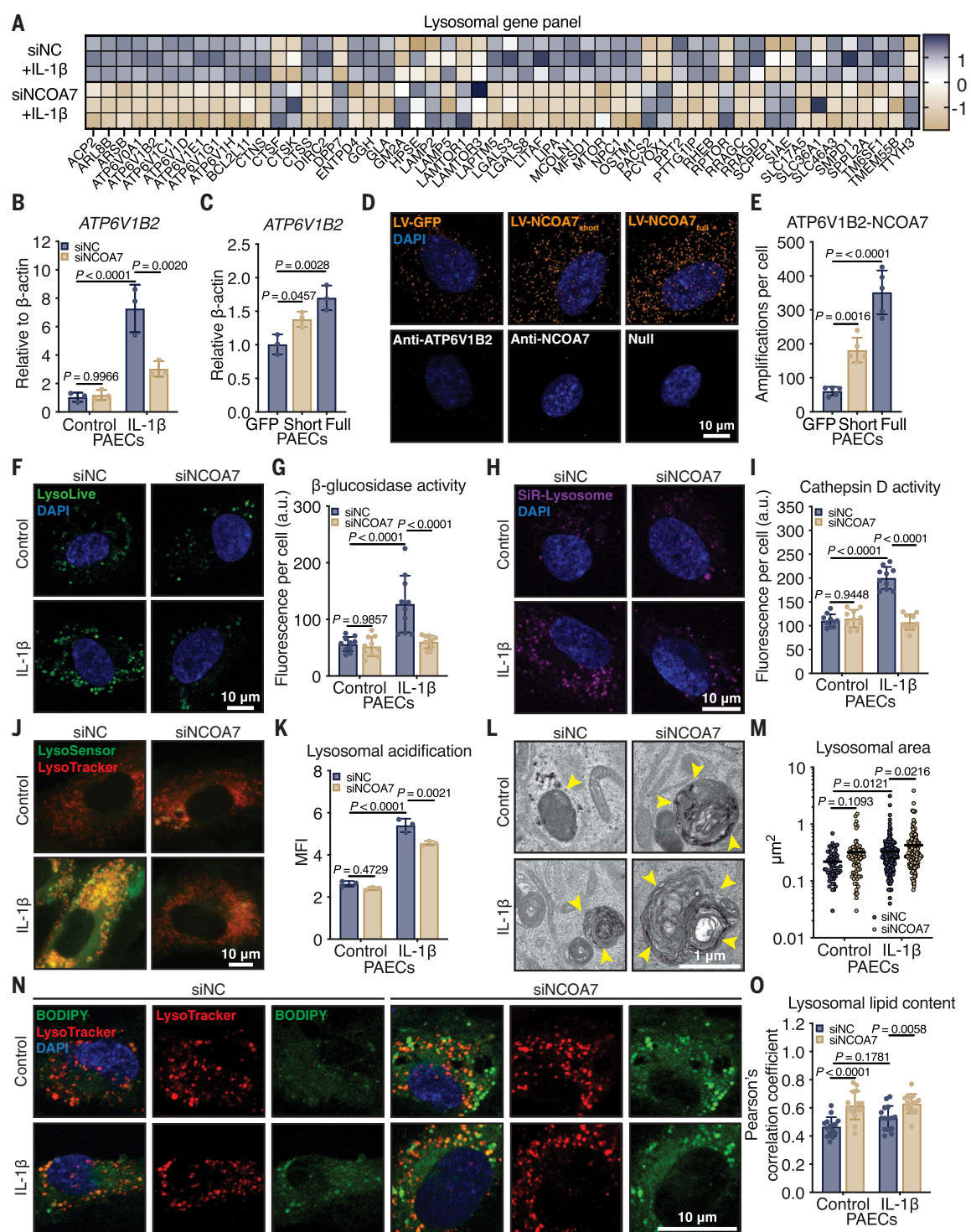
Alterations in lysosomal trafficking affect sterol homeostasis (50). Correspondingly, transcriptomic analysis of NCOA7-deficient human PAECs revealed enrichment and down-regulation of biosynthetic processes related to sterol metabolism (Fig. 3, A and B, red arrows). In a sterol-saturated cell, uptake pathways of extracellular cholesterol are inhibited through reduction of low-density lipoprotein receptor (LDLR) membrane density (51). NCOA7 deficiency in PAECs reduced LDLR expression (Fig. 3C), accompanied by a functional attenuation in the uptake of fluorescently labeled cholesterol (Fig. 3, D and E). Total cholesterol content in NCOA7-deficient PAECs was up-regulated, whereas NCOA7 overexpression reduced cholesterol (Fig. 3, F and G). No differences were detected in post-squalene intermediates in NCOA7-deficient versus NCOA7-replete PAECs (fig. S3, A to N), indicating that NCOA7-dependent modulation of sterol intermediate flux does not rely on de novo cholesterol synthesis. Thus, the down-regulation of sterol metabolism by NCOA7 deficiency is driven primarily by lysosomal alterations of sterol handling rather than de novo synthesis.

To protect against cholesterol accumulation, the cell can either engage in its direct export through transporters or increase its solubility through a series of oxidative steps. Accordingly, deficiency of NCOA7 up-regulated cholesterol 25-hydroxylase (CH25H)—an oxysterol-generating enzyme that increases cholesterol solubility (Fig. 3H and fig. S3O). CH25H was also up-regulated with localization to the endothelium in the pulmonary vessels of proinflammatory rodent models of PAH and PAH patients (Fig. 3, I to N; fig. S3, P and Q; and movies S7 and S8). These data established a central role for NCOA7 in the maintenance of sterols in PAECs and in diseased endothelium *in vivo*.

Induced endothelial generation of oxysterols and downstream bile acid derivatives

To corroborate whether the observed up-regulation of CH25H enhanced oxysterol production, we performed targeted lipidomic analysis using liquid chromatography–mass spectrometry (LC-MS). NCOA7 suppression in human PAECs exposed to IL-1 β up-regulated 25-hydroxycholesterol (25HC), 27-hydroxycholesterol (27HC), and autoxidation-generated 7 α -hydroxycholesterol (Fig. 3, O to Q). These oxysterols are metabolized

Fig. 2. NCOA7 deficiency results in lysosomal dysfunction and lipid accumulation under proinflammatory conditions. (A) Transcriptomic analysis of PAECs under IL-1 β subjected to RNAi against control or NCOA7 ($n = 3$ replicates per group). Z-score is indicated as positive in blue and negative in gold. Identified lysosomal genes have an FDR-corrected P value < 0.05 . (B) Expression of ATP6V1B2 under siNCOA7 by means of RT-qPCR ($n = 3$ replicates per group). (C) Expression of ATP6V1B2 with lentiviral delivery of control [lentiviral green fluorescent protein (LV-GFP)], NCOA7_{short}, or NCOA7_{full} isoforms ($n = 3$ replicates per group). Data analyzed by means of one-way ANOVA. (D) Association of the V-ATPase subunit ATP6V1B2 with NCOA7 measured by means of proximity ligation assay (orange). (Bottom) Control images of ATP6V1B2, NCOA7, or neither antibody. (Top) Dual incubation of ATP6V1B2 and NCOA7 antibodies with lentiviral transduction of GFP control, NCOA7_{short}, or NCOA7_{full}. (E) Quantification of amplified signal per cell ($n = 5$ cells per group). Data were analyzed by means of one-way ANOVA. (F) Lysolive probe (green) reflecting β -galactosidase activity and thus lysosomal acidification. (G) Quantified as fluorescence per cell ($n = 10$ cells per group).



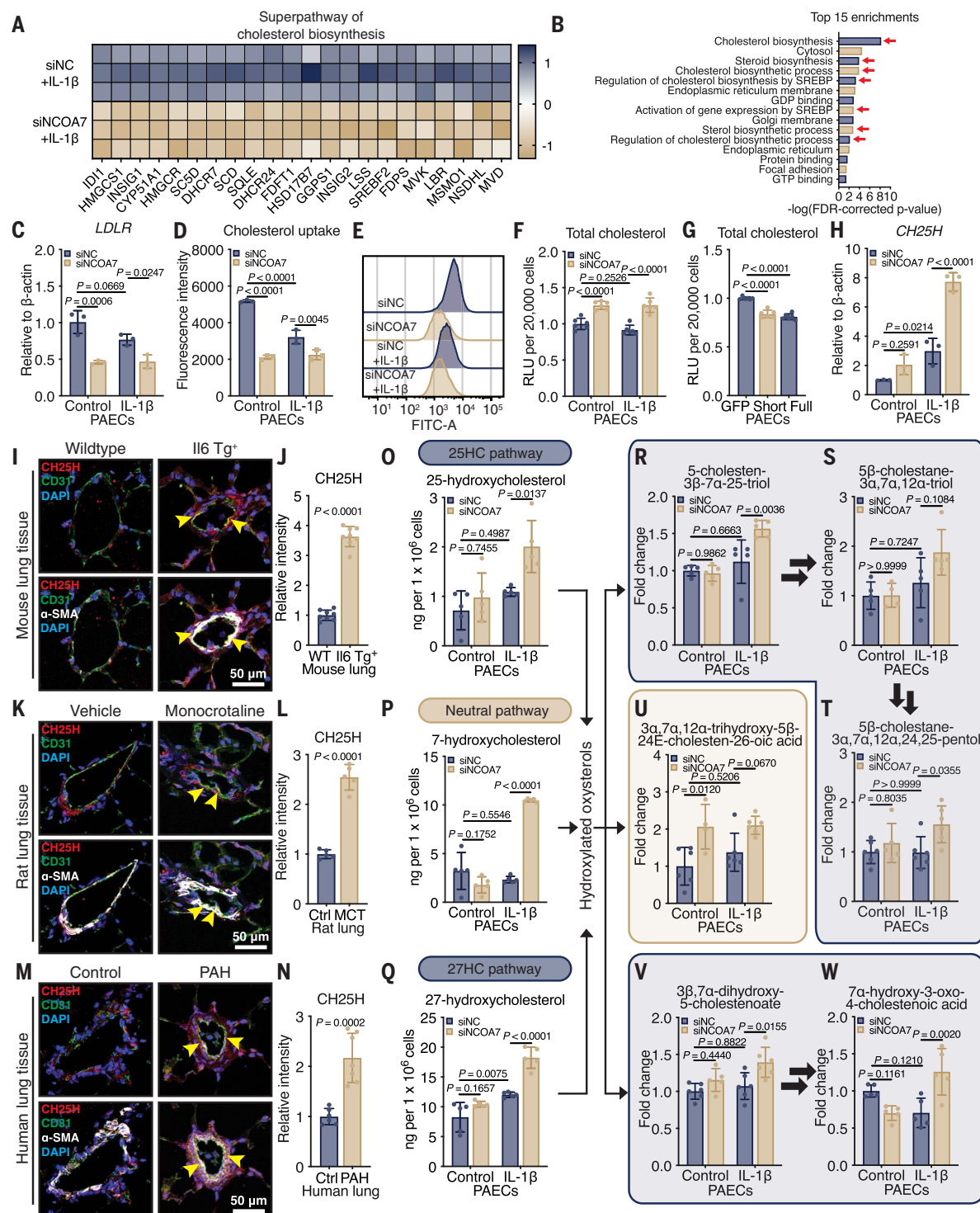


Fig. 3. NCOA7 deficiency reprograms sterol metabolism to up-regulate oxysterols and bile acids. (A) Transcriptomic analysis of PAECs under IL-1 β subjected to RNAi against control or NCOA7 ($n = 3$ replicates per group). Z-score is indicated as positive in blue and negative in gold. Identified cholesterol metabolism genes have an FDR-corrected P value < 0.05 . (B) Gene set enrichment analysis of top 15 pathways by FDR-adjusted P value with a majority related to sterol metabolism and homeostasis (indicated with red arrows). (C) Expression of LDLR under IL-1 β subjected to RNAi against control or NCOA7 ($n = 3$ replicates per group). (D) Fluorescence intensity of tagged NBD-cholesterol uptake ($n = 3$ replicates per group). (E) Flow cytometric plot of fluorescently

tagged nitrobenzodiazepine (NBD)-cholesterol uptake. (F) Total cholesterol content under IL-1 β subjected to RNAi against control or NCOA7 ($n = 3$ replicates per group). (G) Total cholesterol content under IL-1 β subjected to lentiviral overexpression of GFP, NCOA7_{short}, or NCOA7_{full}. Data analyzed by means of one-way ANOVA ($n = 6$ replicates per group). (H) Expression of CH25H in PAECs under IL-1 β subjected to RNAi against control or NCOA7 by means of RT-qPCR ($n = 3$ replicates per group). (I) IF staining for CH25H (red with yellow arrowheads), CD31 $^+$ ECs (green), α -SMA $^+$ smooth muscle cells (white), and DAPI-stained nuclei (blue) in the pulmonary vessels of wild-type versus II6 Tg $^+$ mice. (J) Quantification of CH25H in pulmonary vessels ($n = 8$ mice per group). Student's t test. (K) IF

staining for CH25H (red with yellow arrowheads), CD31⁺ ECs (green), α -SMA⁺ smooth muscle cells (white), and DAPI-stained nuclei (blue) in the pulmonary vessels of control versus monocrotaline rats. (L) Quantification of CH25H in pulmonary vessels ($n = 5$ rats per group). Student's *t* test. (M) IF staining for CH25H (red with yellow arrowheads), CD31⁺ ECs (green), α -SMA⁺ smooth muscle cells (white), and DAPI-stained nuclei (blue) in the pulmonary vessels of healthy human controls versus PAH patients. (N) Quantification of CH25H in pulmonary vessels ($n = 6$ to 7 patients per group). Student's *t* test. (O) Targeted quantification of 25-hydroxycholesterol by means of LC-MS ($n = 5$ replicates per group). (P) Targeted quantification of 7-hydroxycholesterol by means of LC-MS ($n = 5$ replicates per group). (Q) Targeted quantification of 27-hydroxycholesterol by means of LC-MS ($n = 5$ replicates per group). (R) Unbiased bile acid quantification of 5-cholest-3 β -7 α -25-triol

by means of LC-MS ($n = 4$ to 6 replicates per group). (S) Unbiased bile acid quantification of 5 β -cholestane-3 α ,7 α ,12 α -triol by means of LC-MS ($n = 4$ to 6 replicates per group). (T) Unbiased bile acid quantification of 5 β -cholestane-3 α ,7 α ,12 α ,24,25-pentol by means of LC-MS ($n = 4$ to 6 replicates per group). (U) Unbiased bile acid quantification of 3 α ,7 α ,12 α -trihydroxy-5 β -24E-cholest-26-oic acid by means of LC-MS ($n = 4$ to 6 replicates per group). (V) Unbiased bile acid quantification of 3 β ,7 α -dihydroxy-5-cholestenoate by means of LC-MS ($n = 4$ to 6 replicates per group). (W) Unbiased bile acid quantification of 7 α -hydroxy-3-oxo-4-cholestenoic acid (7HOCA) by means of LC-MS ($n = 4$ to 6 replicates per group). Metabolites are organized by proposed pathways in the shaded boxes. Black arrows indicate proposed sequential metabolite pathways. All data were analyzed by means of two-way ANOVA unless otherwise specified and presented as mean \pm SD.

into downstream bile acid derivatives through incompletely understood mechanisms (52). Accordingly, *NCOA7* suppression up-regulated several downstream bile acid derivatives in sequential pathways (35). For example, 5-cholest-3 β -7 α -25-triol and its downstream metabolite 5 β -cholestane-3 α ,7 α ,12 α ,24,25-pentol (Fig. 3, R to T) were up-regulated in *NCOA7*-deficient PAECs. The derivative bile acid 3 α ,7 α ,12 α -trihydroxy-5 β -24E-cholest-26-oic acid was also up-regulated by *NCOA7* deficiency but not with additional inflammatory trigger (Fig. 3U). In another metabolite cascade, 3 β ,7 α -dihydroxy-5-cholestenoate and its downstream derivative 7 α -hydroxy-3-oxo-4-cholestenoic acid (7HOCA) were up-regulated (Fig. 3, V and W) in *NCOA7*-deficient PAECs. Thus, consistent with the up-regulation of the oxysterol-generating enzyme CH25H (Fig. 3H), *NCOA7* deficiency induced production of numerous oxidized cholesterol metabolites and downstream bile acids in PAECs.

Endothelial dysfunction through oxysterol generation

Given the immunomodulatory functions of oxysterols in endothelium (53), we sought to determine whether *NCOA7* deficiency relied on oxysterols to promote EC dysfunction. *NCOA7* deficiency augmented the IL-1 β -dependent induction of vascular cellular adhesion molecule 1 (*VCAM1*)—a surrogate of endothelium immunoactivation (Fig. 4, A and B). These findings were consistent with the up-regulation of endothelial *VCAM1* seen in human PAH (movies S9 and S10). Conversely, *NCOA7* overexpression reversed *VCAM1* expression (Fig. 4, C and D). Inhibition of CH25H induction under *NCOA7* deficiency prevented *VCAM1* expression (Fig. 4, E and F). Correspondingly, either in the presence or absence of IL-1 β , *NCOA7* suppression in PAECs augmented leukocyte (Fig. 4G) attachment, whereas *NCOA7* overexpression reduced attachment (Fig. 4H). CH25H suppression reversed the augmented immune cell attachment driven by *NCOA7* deficiency (Fig. 4I). A similar pattern was observed for monocyte attachment (Fig. 4, J to L). These data demonstrate that *NCOA7* deficiency was dependent on CH25H-dependent oxysterol generation to induce PAEC inflammatory pathophenotypes.

Downstream of inflammation, *NCOA7* deficiency in PAECs abrogated IL-1 β -mediated apoptosis while simultaneously enhancing proliferative capacity (fig. S4, A and B). *NCOA7* facilitated PAEC apoptosis under proinflammatory conditions (fig. S4C) and attenuated proliferation with more pronounced inhibition under IL-1 β (fig. S4D). Inhibition of CH25H up-regulation reversed the attenuation of apoptosis but augmented rather than reversed proliferation (fig. S4, E and F). Our findings demonstrate that *NCOA7* deficiency promotes a proinflammatory, proproliferative, and antiapoptotic condition distinct from that seen with simply IL-1 β exposure alone and a pathologic endothelial state more closely consistent with PAH (54, 55). Furthermore, across its regulatory roles of inflammation and apoptosis, *NCOA7* depends on the CH25H-dependent generation of certain oxysterols and bile acids.

To determine whether downstream bile acids are sufficient to immunoactivate the endothelium, 7HOCA was directly applied to PAECs in culture. Displaying its proinflammatory nature, 7HOCA up-regulated *VCAM1* (Fig. 4, M and N), thus promoting adhesion of both leukocytes and monocytes to a PAEC monolayer (Fig. 4, O and P). Representative of upstream oxysterol metabolites, the direct application of 25HC and downstream derivatives, such as the triol and tetrol (Fig. 3, O and R), similarly up-regulated *VCAM1* and enhanced immune cell adhesion to a PAEC monolayer (fig. S4, G to Q). Thus, these findings demonstrate that oxysterol-generating enzymes and their downstream sterol species are necessary and sufficient for mediating immune activation of the *NCOA7*-deficient pulmonary endothelium.

Loss of *NCOA7* and outcomes

Orotracheal delivery of 7HOCA worsens PAH *in vivo*

To determine whether the presence of *NCOA7* protects against EC immunoactivation and controls PAH severity, we used an *IIL* transgenic (Tg⁺) mouse to elicit pulmonary inflammation as a model of angioproliferative PAH (56). A mouse in which *Ncoa7* was wholly deleted was crossed onto *IIL* Tg⁺ mice to determine whether loss of *NCOA7* would worsen

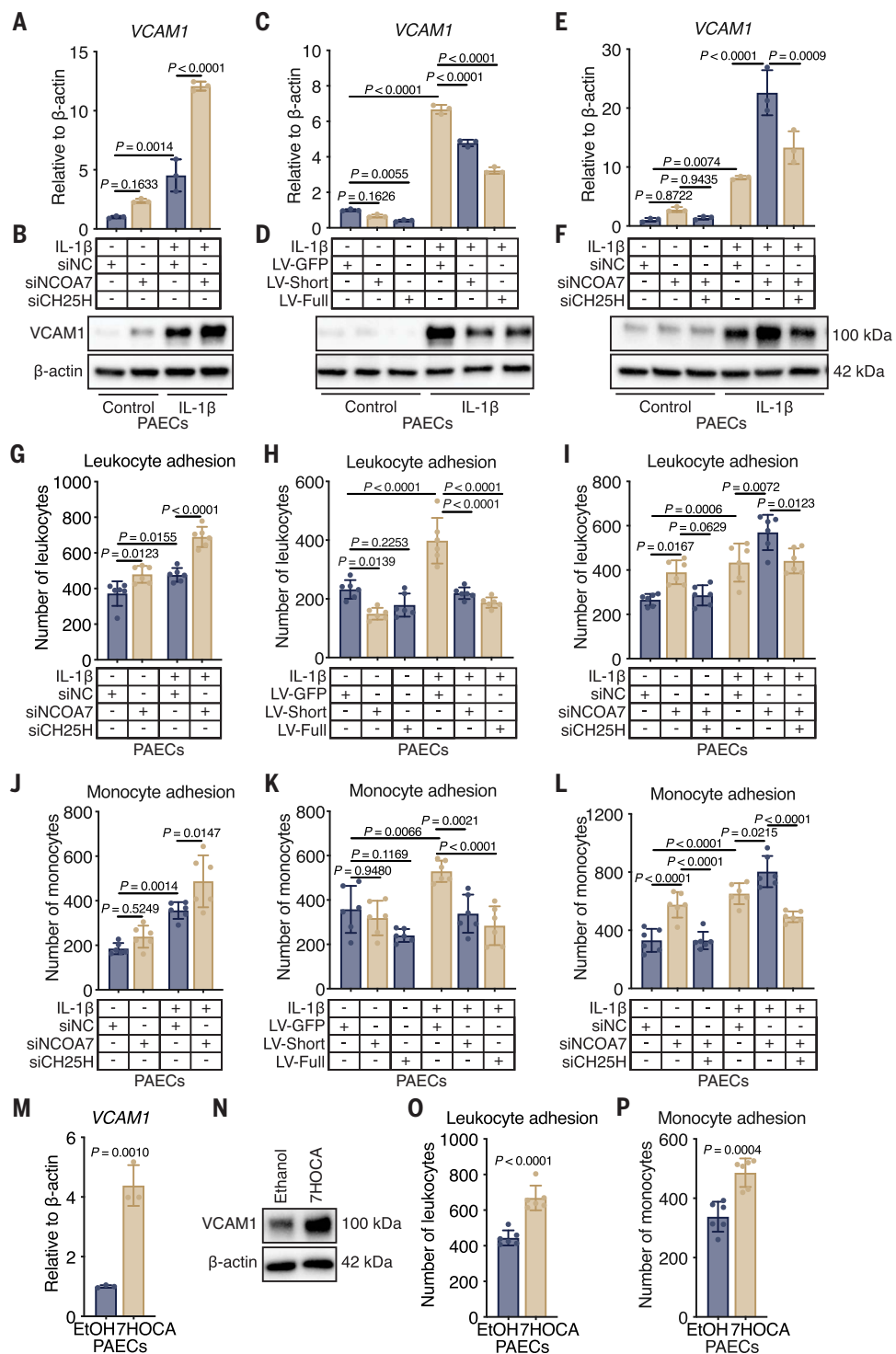
indices of PH *in vivo* (Fig. 5A). Echocardiographic assessment excluded any alterations in left ventricular (LV) function (fig. S5, A to D).

Ncoa7-null mice displayed elevated CH25H expression in pulmonary arterioles, which corresponded to increased *VCAM1* expression, CD11b⁺ monocyte infiltration, and worsened vascular remodeling (Fig. 5, B to F). The up-regulation of CH25H was accompanied by elevated plasma levels of 7HOCA and the downstream tetrol species of 25HC (Fig. 5, B, C, and G, and fig. S5, E to H). These findings corresponded with the oxysterol and bile acid plasma signatures associated with PAH severity in humans (35) and our studies of cultured PAECs (Fig. 3). To more precisely detect the variety of ways that right ventricular (RV) dysfunction could manifest with inflammation (57), we studied three indices reflecting differing yet complementary aspects of RV dysfunction: RV fractional area change (RVFAC; a measure of global RV systolic function), tricuspid annular plane systolic excursion (TAPSE; a measure of longitudinal RV systolic function), and Fulton's index (a measure of global, concentric RV remodeling). *Ncoa7*-null mice displayed increased Fulton's index and reduced RVFAC with no change in TAPSE (Fig. 5, H to J). Correspondingly, *Ncoa7*-null mice demonstrated increased right ventricular systolic pressure (RVSP) when we used invasive catheterization (Fig. 5K).

To assess whether endothelial *Ncoa7* deficiency drives disease, we used a validated 7C1 oligomeric lipid nanoparticle system to deliver silencing RNA against *Ncoa7* versus control to the endothelium by means of tail vein injection in *IIL* Tg⁺ mice (Fig. 5L) (58). Echocardiography excluded LV or cardiac output (CO) alterations (fig. S5, I to L). In 7C1:si*Ncoa7* *IIL* Tg⁺ mice, *NCOA7* was suppressed in pulmonary arteriolar endothelium as compared with smooth muscle (Fig. 5, M to O; fig. S5M; and movies S11 and S12). Loss of *Ncoa7* up-regulated CH25H and *VCAM1*, leading to CD11b⁺ monocyte infiltration, more severe vessel remodeling, worsened RV function (according to Fulton's index, RVFAC, and TAPSE), and more severe hemodynamic compromise of RVSP (Fig. 5, P to W; fig. S5M; and movies S13 to S18).

Fig. 4. The NCOA7-CH25H axis drives pulmonary endothelial immunoactivation.

(A) VCAM1 expression by means of RT-qPCR under RNAi against NCOA7 ($n = 3$ replicates per group). (B) VCAM1 expression by means of immunoblot under RNAi against NCOA7 ($n = 3$ replicates per group). (C) VCAM1 expression by means of RT-qPCR under lentiviral delivery of NCOA7_{short} or NCOA7_{full} ($n = 3$ replicates per group). (D) VCAM1 expression by means of immunoblot under lentiviral delivery of NCOA7_{short} or NCOA7_{full} ($n = 3$ replicates per group). (E) VCAM1 expression by means of RT-qPCR under RNAi against NCOA7 and CH25H ($n = 3$ replicates per group). (F) VCAM1 expression by means of immunoblot under RNAi against NCOA7 and CH25H ($n = 3$ replicates per group). (G) Leukocyte adhesion under RNAi against NCOA7 ($n = 6$ replicates per group). (H) Leukocyte adhesion under lentiviral delivery of NCOA7_{short} or NCOA7_{full} ($n = 6$ replicates per group). (I) Leukocyte adhesion under RNAi against NCOA7 and CH25H ($n = 6$ replicates per group). (J) Monocyte adhesion under RNAi against NCOA7 ($n = 6$ replicates per group). (K) Monocyte adhesion under lentiviral delivery of NCOA7_{short} or NCOA7_{full} ($n = 6$ replicates per group). (L) Monocyte adhesion under RNAi against NCOA7 and CH25H ($n = 6$ replicates per group). (M) VCAM1 expression by means of RT-qPCR under control (ethanol) versus 7HOCA (50 μ M) for 24 hours ($n = 3$ replicates per group; Student's *t* test). (N) VCAM1 expression by means of immunoblot under control (ethanol) versus 7HOCA (50 μ M) for 24 hours ($n = 3$ replicates per group; Student's *t* test). (O) Leukocyte adhesion in 7HOCA-treated PAECs compared with ethanol controls ($n = 6$ replicates per group; Student's *t* test). (P) Monocyte adhesion in 7HOCA-treated PAECs compared with ethanol controls ($n = 6$ replicates per group; Student's *t* test). All data were analyzed by means of two-way ANOVA unless otherwise specified and presented as mean \pm SD.



Last, to assess the pathogenicity of 7HOCA directly, we used a chronically hypoxic mouse model with serial, orotracheal deliveries of either normal saline or 7HOCA (Fig. 5X) and confirmed with echocardiography no alterations in LV function (fig. S5, N to Q). As expected, delivery of 7HOCA up-regulated immunoactivation of the endothelium, as indicated by increased VCAM1 and vascular CD11b⁺ monocyte infiltration (Fig. 5, Y to AA). Consistent with

genetic deletion of *Ncoa7*, 7HOCA worsened PAH, as reflected by increased pulmonary arteriolar remodeling, worsened RV dysfunction according to RVFAC and TAPSE (but unchanged Fulton's index), and increased RVSP (Fig. 5, AC to AF). Taken together, our data demonstrated that both global and endothelial-specific loss of *Ncoa7* or the direct delivery of the proinflammatory sterol 7HOCA were sufficient to promote and worsen PH. Moreover, all models

demonstrated RV dysfunction; however, we observed specific differences regarding which RV functional indices were altered, suggesting pleiotropic mechanisms through which inflammation affects cardiac and vascular remodeling.

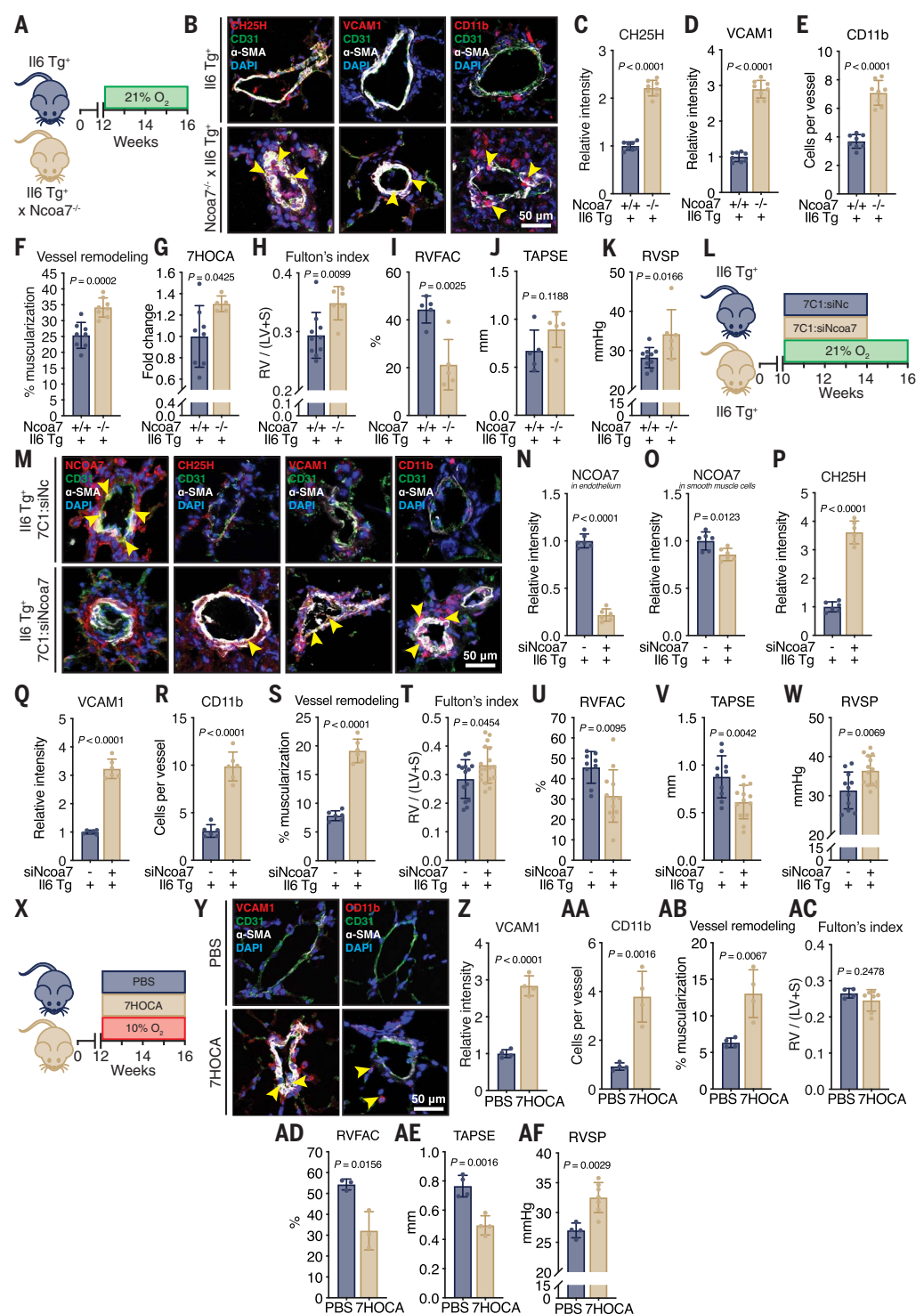
Oxysterols and bile acids predict morbidity and mortality in clinical PAH

Underscoring the clinical importance of this mechanism in controlling disease severity, we

Fig. 5. Genetic loss of Ncoa7 and the orotracheal delivery of 7HOCA worsens PAH in vivo. (A) Ncoa7-null mice crossed onto the II6 Tg⁺ PAH model. (B) Pulmonary arterioles from II6 Tg⁺ versus Ncoa7^{-/-} × II6 Tg⁺ mice stained for a target protein (CH25H, VCAM1, or CD11b; red with yellow arrowheads), the endothelial layer (CD31; green), the smooth muscle layer (α -SMA; white), and nuclear counterstain (DAPI; blue). (C to F) Quantification of (C) CH25H relative intensity, (D) VCAM1 relative intensity, (E) CD11b⁺ cells, and (F) vessel remodeling by means of percent muscularization in the pulmonary arterioles of II6 Tg⁺ versus Ncoa7^{-/-} × II6 Tg⁺ mice ($n = 8$ mice per group). (G) 7HOCA fold change, (H) Fulton's Index, (I) RVFAC, (J) TAPSE, and (K) RVSP of II6 Tg⁺ versus Ncoa7^{-/-} × II6 Tg⁺ mice ($n = 6$ to 10 mice per group). (L) II6 Tg⁺ mice were serially injected in the tail vein with either 7C1 nanoparticle encapsulated mouse siRNA against negative control or Ncoa7 (1 mg/kg) starting at 10 weeks of age every 5 days for a total of five doses and were euthanized at 16 weeks. (M) Pulmonary arterioles from siNC:7C1 II6 Tg⁺ versus siNCOA7:7C1 II6 Tg⁺ mice stained for a target protein (NCOA7, CH25H, VCAM1, or CD11b; red with yellow arrowheads), the endothelial layer (CD31; green), the smooth muscle layer (α -SMA; white), and nuclear counterstain (DAPI; blue). (N to S) Quantification of the relative intensity of (N) NCOA7 in endothelium, (O) NCOA7 in smooth muscle cells, (P) CH25H, (Q) VCAM1, (R) the number of CD11b⁺ cells per vessel, or (S) the degree of vessel muscularization defined by α -SMA layer thickness to total vessel diameter. ($n = 6$ mice per group). (T) Fulton's Index, (U) RVFAC, (V) TAPSE, and (W) RVSP of 7C1:siNc II6 Tg⁺ versus 7C1:siNcoa7 II6 Tg⁺ mice ($n = 9$ to 18 mice per group). (X) Mice received orotracheal delivery of either PBS or 7HOCA (10 mg/kg) for 4 weeks under hypoxic (10% O₂) conditions and were euthanized at 16 weeks. (Y) Pulmonary arterioles from PBS versus 7HOCA mice stained for a target protein (VCAM1, or CD11b; red with yellow arrowheads), the endothelial layer (CD31; green), the smooth muscle layer (α -SMA; white), and nuclear counterstain (DAPI; blue). (Z to AB) Quantification of the relative intensity of (Z) VCAM1, (AA) the number of CD11b⁺ cells per vessel, or (AB) the degree of vessel muscularization defined by α -SMA layer thickness to total vessel diameter ($n = 4$ mice per group). (AC) Fulton's Index, (AD) RVFAC, (AE) TAPSE, and (AF) RVSP of mice receiving orotracheal PBS or 7HOCA ($n = 3$ to 7 mice per group). All data were analyzed by means of Student's *t* test unless otherwise specified and presented as mean ± SD.

identified a plasma signature inclusive of the same NCOA7-dependent sterols and bile acids associated with PAH mortality (adjusted $P < 1.1 \times 10^{-6}$). In our companion study (35)—by means of an unbiased, metabolome-wide asso-

ciation study from the multicenter PAH Biobank cohort ($n = 2756$ patients)—Alotaibi *et al.* identified 13 distinct plasma oxysterols and bile acids that best predicted 4-year mortality in PAH [area under the curve (AUC) 73%; 95% confi-



dence interval (CI), 68% to 78%] (35). Of these 13 oxysterols and bile acids, five were either the same metabolites or were metabolic precursors or derivatives of those up-regulated in NCOA7-deficient PAECs (Fig. 3, T, U, and W) or in the

plasma of *Ncoa7*-deficient mice (Fig. 5G and fig. S5H). In a single-center PAH cohort from the University of Pittsburgh Medical Center (UPMC-a, $n = 116$ patients) (table S1), higher plasma concentrations of these single oxysterols and bile acids were each associated with increased mortality or transplantation risk, after adjusting for age, sex, and prostacyclin therapy (Fig. 6A and table S4) (35). Associations of these same metabolites with elevated mortality hazard ratios were consistent across two additional independent multicenter PAH cohorts, as reported in Alotaibi *et al.* (35). These findings emphasize the clinical importance of NCOA7-dependent oxysterols and bile acids in controlling PAH severity, linking lysosome-dependent inflammation with metabolome-wide signals in PAH.

Intronic SNP rs11154337 controls RelA/p65 binding to the noncanonical promoter of NCOA7 and is associated with PAH disease severity and mortality

Our findings thus far defined NCOA7 as a homeostatic brake in proinflammatory conditions that preserves lysosomal activity and sterol trafficking to attenuate EC immunoactivation in PAH. On the basis of the role of single-nucleotide polymorphisms (SNPs) in the regulation of gene promoter activity (59), we sought to determine whether pathogenic NCOA7 deficiencies could result from genetic, SNP-dependent control of NCOA7 expression and its downstream function (Figs. 1 to 5). First, we surveyed annotated SNPs on the basis of their proximity to the canonical and noncanonical promoters and high levels of epigenetic marks that indicate elevated transcriptional activity. In doing so, we found a candidate SNP—rs11154337 (GRCh38, chr6:125922445)—located near an intronic region proximal to the noncanonical promoter of *NCOA7* and carrying a substantial burden of histone modifications (37). Second, given the tandem regulation of both short- and full-length isoforms of NCOA7 in PAH (Fig. 1), we sought to discern any regulatory function of this SNP by means of positional backfolding onto the canonical promoter. Through analysis of high-throughput chromatin conformation capture (3C) on human umbilical vein ECs [Gene Expression Omnibus (GEO) IDs GSM3438650 and GSM3438651] from the 3D-genome Interaction Viewer & database (3DIV) (60), long-range interactions (>120 kb) were identified between SNP rs11154337 and the canonical promoter region of *NCOA7* (fig. S6A). 3C analysis performed on human PAECs demonstrated an interaction between the genomic loci encompassing SNP rs11154337 and the *NCOA7* transcription start site (fig. S6, B and C). Furthermore, ChIP against RelA/p65 revealed an enrichment for the SNP-containing region, supporting the presence of a p65 protein-SNP complex (fig. S6D).

We then sought to determine whether this SNP was associated with disease severity and mortality, using two independent PAH cohorts (fig. S6E). First, we analyzed a single-center PAH cohort of European-descent subjects from the University of Pittsburgh Medical Center with adjustments for age, sex, and vasodilator use (UPMC-b; $n = 93$ patients) (Table 1). The G allele was associated with a significantly longer 6-min walk distance [$P = 0.0130$; $\beta = 66.90$, 95% CI (14.45–119.36)] (fig. S6F). Survival was significantly increased in patients who carried G alleles [$P = 0.009$; hazard ratio = 0.54, 95% CI (0.34–0.86)] (Fig. 6B). In a second, multicenter PAH cohort of European-descent derived both from prospective recruitment and from retrospective inclusion of PAH patients from the Sitaxsentan To Relieve Impaired Exercise (STRIDE) trial (STRIDE+; $n = 630$ patients) (Table 1) (61), we validated that the G allele conferred a substantial survival benefit after adjustments for age, sex, PAH type, type of study inclusion, World Health Organization (WHO) functional classification, and vasodilator use [$P = 0.0002$, hazard ratio = 0.49, 95% CI (0.34–0.71)] (Fig. 6C). Further adjustment for pulmonary vascular resistance (PVR) had no effect on the survival benefit in the UPMC-b cohort [$P = 0.004$; hazard ratio = 0.51, 95% CI (0.32–0.81)] and had only partial effect in the STRIDE+ cohort [$P = 0.005$, hazard ratio = 0.64, 95% CI (0.47–0.88)], suggesting that PVR alone cannot fully explain the association. Thus, analysis of genomic, metabolomic, and clinical datasets across cohorts of PAH patients demonstrated the presence of interconnected activities between NCOA7 and SNP rs11154337 with glucuronidated oxysterols and clinical outcomes of PAH.

Identification of an allele-specific SNP and its downstream pathogenic functions

We then sought to determine whether this SNP controls NCOA7 expression, lysosomal activity, and the production of oxysterol and bile acid metabolites to modulate EC behavior. To study the cellular and biological activity of SNP rs11154337 embedded near the noncanonical *NCOA7* promoter, we generated a set of genetically matched, isogenic inducible pluripotent stem cell (iPSC) lines with the allelic variants of SNP rs11154337 by means of CRISPR-Cas9 gene editing (C/C versus C/G genotypes) (Fig. 6D and fig. S6G). The iPSCs were then differentiated into ECs (iPSC-ECs) (fig. S6H) (62), and iPSC-ECs exhibited marked enrichment of EC markers and displayed angiogenic potential (fig. S6, H and I).

Consistent with interactions of SNP rs11154337 with promoters of both short- and full-length *NCOA7*, C/G versus C/C iPSC-ECs displayed higher transcript expression of both isoforms and preferential up-regulation of short-length NCOA7, demonstrating that the G allele increases *NCOA7* levels (Fig. 6, E and F, and fig.

S6J). Consistent with our prior findings of *NCOA7* manipulation in PAECs, iPSC-ECs carrying the G allele—and thus higher *NCOA7* expression—displayed a concomitant increase in its binding partner *ATP6VIB2* and subsequently lower lysosomal pH, as demonstrated by enhanced cleavage of SiR-Lysosome (Fig. 6, G to I). Moreover, the presence of the G allele prevented lysosomal hypertrophy in comparison with the iPSC-EC line homozygous for the C allele, indicating maintenance of proper lysosomal acidification and resultant sterol homeostasis (Fig. 6J and fig. S6K).

Reduced *NCOA7* expression in the homozygous C allele line resulted in higher sterol content and drove higher expression of *CH25H* and its metabolite 25HC (Fig. 6, K to O), the upstream precursor for oxidized species such as 7HOCA. With greater production of 25HC, the homozygous C allele iPSC-line displayed elevated EC immunoactivation, reflected by enhanced VCAM1 expression and immune-cell adhesion (Fig. 6, P to S). Thus, consistent with the association of the G allele of SNP rs11154337 as protective against oxysterol production and PAH severity, the G allele increased *NCOA7* expression and its downstream modulation of lysosomal acidification, oxysterol generation, and EC immunoactivation.

NCOA7 as therapeutic target

Structural modeling identifies an activator of NCOA7

To identify a small-molecule activator of NCOA7, we performed structure-based computations composed of three parts: druggability simulations, pharmacophore modeling, and virtual screening (Fig. 7, A to C). Druggability simulations were carried out by using the model structure of NCOA7 in the presence of explicit water and probe molecules representative of drug-like fragments (63), in which probe molecules were run to determine a molecular pocket (Fig. 7A, cyan spheres) and hinge residues that are critical in mediating protein functional dynamics (fig. S7, A and B; in-depth discussion is available in the supplementary text).

Pharmacophore modeling identified high-affinity residues (Fig. 7B) at the molecular pocket, which were screened against the ZINC (64) and MolPort small-molecule libraries to obtain a ranked ensemble of compounds. Subsequently, top scoring compounds were further investigated, in which pilot screening suggested that compound (6,7-dihydroxy-2-oxo-2H-chromen-4-yl) methyl 4-oxo-3-phenyl-3,4-dihydrophthalazine-1-carboxylate [MolPort-004-267-958; herein called 958 (Fig. 7C)] was an activator rather than an inhibitor of NCOA7. As such, further investigation on the binding behavior of 958 through molecular dynamics simulations was performed.

Refinement of the activator 958 to optimize binding affinity

Molecular dynamics simulations identified the most critical functional groups and interactions

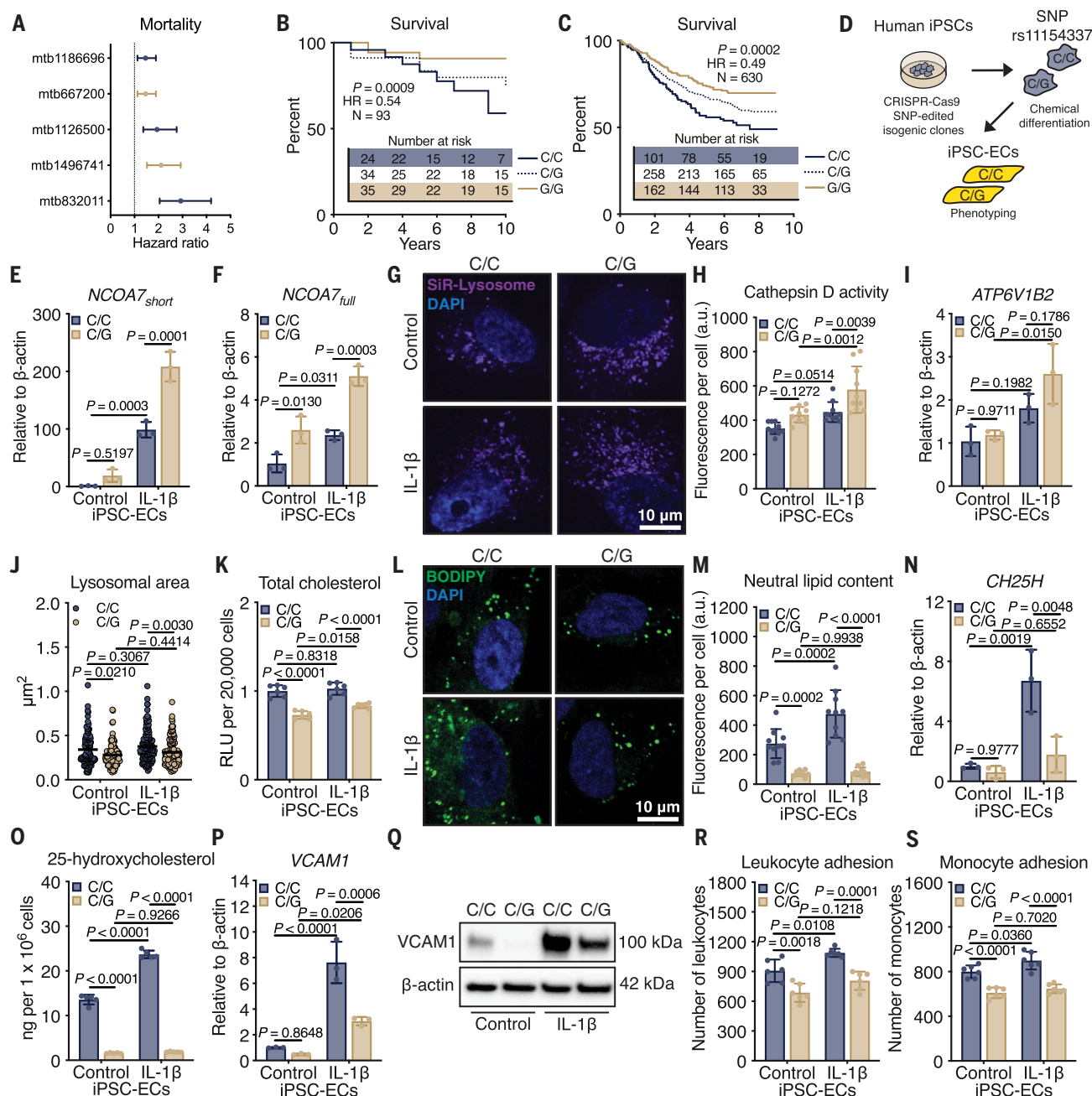


Fig. 6. The G allele of SNP rs11154337 prevents lysosomal lipid accumulation and attenuates oxysterol-mediated immunoactivation in iPSC-ECs.

(A) Metabolites identified in *NCOA7*-deficit PAECs or in the plasma of *Ncoa7*-deficient mice individually were associated with higher mortality in PAH patients in the UPMC-a cohort ($n = 116$ patients; Cox regression with multivariate adjustment; P value cutoff < 0.01). (B and C) Allelic variants of SNP rs11154337 and their clinical readouts of 6-min walk distance (6MWD) and survival in PAH patients in the UPMC-b cohort ($n = 93$ patients) and STRIDE+ cohort ($n = 630$ patients). (D) Schematic of iPSC-EC production. (E) *NCOA7_{short}* and (F) *NCOA7_{full}* expression by means of RT-qPCR in iPSC-ECs under IL-1 β ($n = 3$ replicates per group). (G) IF staining with SiR-Lysosome dye against active cathepsin D and (H) quantification of fluorescence in iPSC-ECs under control or IL-1 β (purple; $n = 10$ cells per group). (I) *ATP6V1B2* expression by means of RT-qPCR in iPSC-ECs under control or IL-1 β ($n = 3$ replicates per group). (J) Transmission electron micrograph quantification of lysosomal area in iPSC-ECs under control or IL-1 β . (K) Total cholesterol content as measured by means of relative luminescence in iPSC-ECs under control or IL-1 β ($n = 6$ replicates per group). (L) IF staining with BODIPY dye against neutral lipids and (M) quantification of fluorescence in iPSC-ECs under control or IL-1 β (green; $n = 10$ cells per group). (N) *CH25H* expression by means of RT-qPCR in iPSC-ECs under control or IL-1 β ($n = 3$ replicates per group). (O) Targeted 25HC quantification by means of LC-MS in iPSC-ECs under control or IL-1 β ($n = 5$ replicates per group). (P) *VCAM1* expression by means of RT-qPCR or (Q) immunoblot in iPSC-ECs under control or IL-1 β ($n = 3$ replicates per group). (R) Leukocyte and (S) monocyte adhesion to iPSC-EC monolayer under control or IL-1 β ($n = 6$ replicates per group). All data were analyzed by means of two-way ANOVA unless otherwise specified and presented as mean \pm SD.

group). (J) Transmission electron micrograph quantification of lysosomal area in iPSC-ECs under control or IL-1 β . (K) Total cholesterol content as measured by means of relative luminescence in iPSC-ECs under control or IL-1 β ($n = 6$ replicates per group). (L) IF staining with BODIPY dye against neutral lipids and (M) quantification of fluorescence in iPSC-ECs under control or IL-1 β (green; $n = 10$ cells per group). (N) *CH25H* expression by means of RT-qPCR in iPSC-ECs under control or IL-1 β ($n = 3$ replicates per group). (O) Targeted 25HC quantification by means of LC-MS in iPSC-ECs under control or IL-1 β ($n = 5$ replicates per group). (P) *VCAM1* expression by means of RT-qPCR or (Q) immunoblot in iPSC-ECs under control or IL-1 β ($n = 3$ replicates per group). (R) Leukocyte and (S) monocyte adhesion to iPSC-EC monolayer under control or IL-1 β ($n = 6$ replicates per group). All data were analyzed by means of two-way ANOVA unless otherwise specified and presented as mean \pm SD.

Table 1. Cohort demographics and clinical characteristics.

UPMC-a cohort (n = 116 patients)	
Demographics	Number (%)
Female	72 (62.1)
Male	44 (37.9)
Clinical characteristics	Median (25–75%)
Age at catheterization (years)	54 (42–64)
Mean right atrial pressure (mmHg)	8.00 (5.00–15.00)
Mean pulmonary artery pressure (mmHg)	44.00 (31.00–54.00)
Pulmonary capillary wedge pressure (mmHg)	9.00 (7.00–12.25)
Cardiac output (liter/min)	4.96 (3.86–6.36)
Cardiac index (liter/min/kg/m ²)	2.79 (2.22–3.18)
Pulmonary vascular resistance (Wood units)	4.82 (3.40–9.99)
UPMC-b cohort (n = 93 patients)	
Demographics	Number (%)
Female	74 (79.6)
Male	19 (20.4)
Clinical characteristics	Median (25–75%)
Age at catheterization (years)	51 (36–60)
Mean right atrial pressure (mmHg)	9.00 (4.50–13.00)
Mean pulmonary artery pressure (mmHg)	51.50 (40.75–60.25)
Pulmonary capillary wedge pressure (mmHg)	10.00 (7.00–14.00)
Cardiac output (liter/min)	4.30 (3.45–5.40)
Cardiac index (liter/min/kg/m ²)	2.30 (1.93–2.84)
Pulmonary vascular resistance (Wood units)	9.70 (5.74–13.11)
STRIDE+ cohort (n = 630 patients)	
Demographics	Number (%)
Female	503 (79.8)
Male	127 (20.2)
Clinical characteristics	Median (25–75%)
Age at catheterization (years)	52.02 (38.98–62.68)
Mean right atrial pressure (mmHg)	7.00 (5.00–11.00)
Mean pulmonary artery pressure (mmHg)	50.00 (38.00–61.00)
Pulmonary capillary wedge pressure (mmHg)	10.00 (7.00–13.00)
Cardiac output (liter/min)	4.30 (3.40–5.50)
Cardiac index (liter/min/kg/m ²)	2.40 (1.96–3.00)
Pulmonary vascular resistance (Wood units)	9.99 (6.00–14.00)

between 958 and the molecular pocket of NCOA7 (Fig. 7C). From these simulations, an analog of 958 was designed, in which the O₁₅ atom of the ester functional group was replaced with N₁₅-H to create an amide functional group, with the resultant compound herein called 958_{ami} (Fig. 7, D and E). Further molecular dynamics simulations were run to compare the parental versus analog structures (958 versus 958_{ami}) and revealed stronger interactions between 958_{ami} and the molecular pocket of NCOA7 (Fig. 7, D and E, orange solid lines, and fig. S8, A to C). This corresponded to a small molecule more stably bound to NCOA7 than the parental compound (fig. S9, A and B; in-depth discussion is available in the supplementary text).

Administration of activator 958_{ami} reverses existing PAH in rats

To assess the downstream molecular functions of NCOA7 activation with 958_{ami}, we performed

a proximity ligation assay to assess ATP6V1B2-NCOA7 interactions. Application of 958_{ami} induced the amplifications per cell, indicating enhancement of ATP6V1B2-NCOA7 lysosomal interactions (Fig. 7, F and G). As such, 958_{ami} enhanced cellular acidification (Fig. 7H), prevented induction of *CH25H* under IL-1 β , and decreased EC immunoactivation as indicated by VCAM1 expression and immune cell adhesion to a monolayer (Fig. 7, I to M, and fig. S10A).

We sought to confirm whether 958_{ami} would protect against endothelial immunoactivation and PAH in vivo. Using the proinflammatory monocrotaline PAH rat model, rodents were injected intraperitoneally with dimethyl sulfoxide (DMSO) or 958_{ami} (7.5 mg/kg) for 10 days after monocrotaline loading (Fig. 7N). Rodents treated with 958_{ami} versus vehicle control did not display appreciable hepatic or renal toxicity or alterations in LV function (fig. S10, B to J). Rats treated with 958_{ami} exhibited decreased

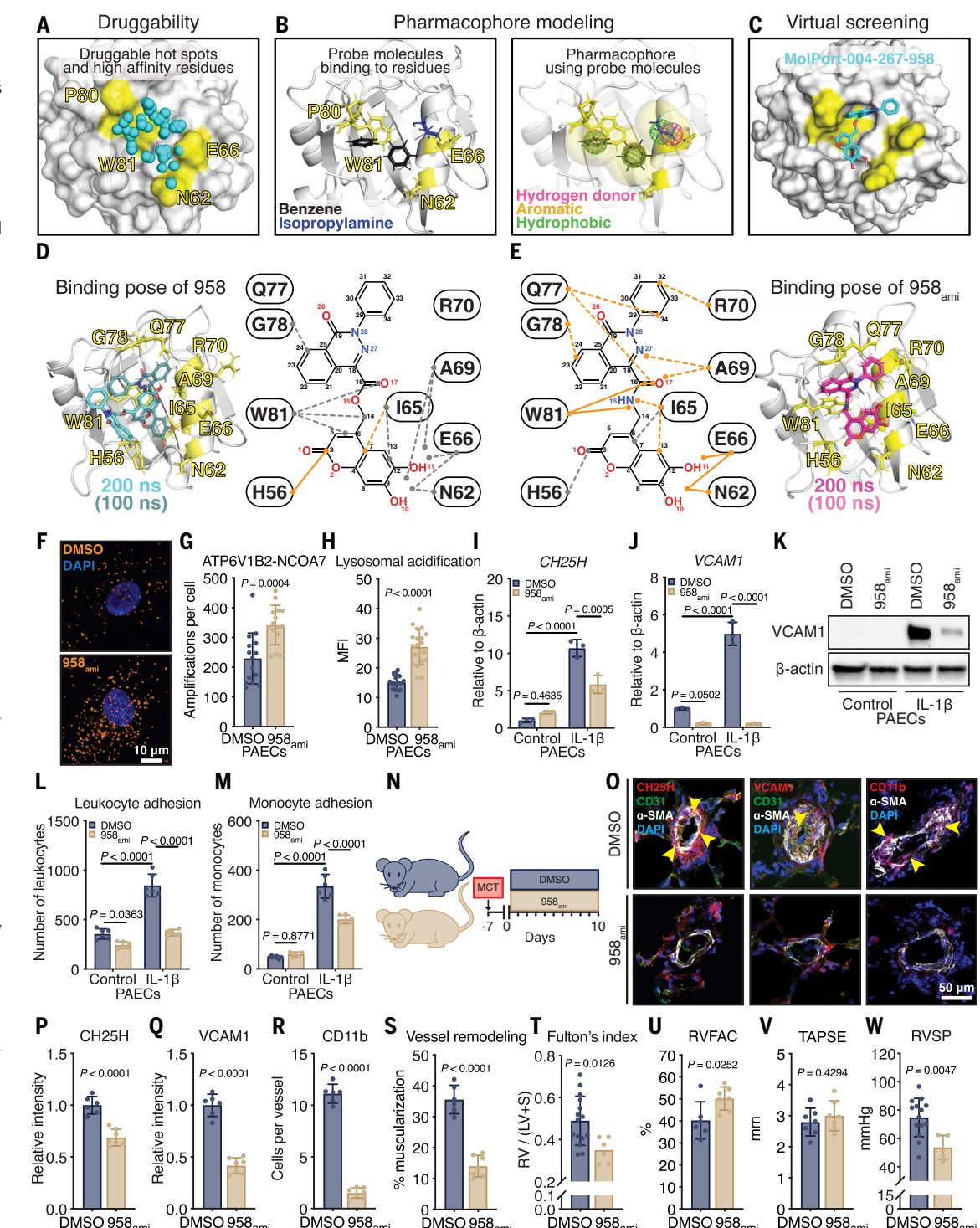
CH25H expression, with a corresponding attenuation in endothelial VCAM1 expression and vascular CD11b⁺ monocyte infiltration (Fig. 7, O to R, and movies S19 to S22). As a result, pulmonary vessels demonstrated decreased muscularization, which corresponded to a reduction in both RV hypertrophy according to Fulton's index, improved RVFAC (without change in TAPSE), and decreased RVSP (Fig. 7, T to W). Overall, these data identified 958_{ami} as a potential therapeutic agent that can reverse PAH pathogenesis.

Discussion

By harnessing large-scale, multidimensional genomic and metabolomic analytics with concomitant mechanistic experimentation, we found that NCOA7 regulates lysosomal activity and EC sterol metabolism to function as a homeostatic brake and prevents oxysterol-induced inflammation, EC dysfunction, and PAH. The G allele at SNP rs11154337 enhances *NCOA7* expression to reduce inflammation in PAH and offers a mechanistic explanation of the genetic association between SNP rs11154337 and PAH mortality as well as the metabolomic association between the oxysterol signature and PAH severity. Our work links fundamental lysosomal biology and oxysterol metabolism to EC behavior, thus guiding development of potential molecular diagnostics and therapeutics in PAH.

The identification of NCOA7 as a primary controller of PAH has broad implications. Previously studied in bacterial (19) and viral invasion (16, 20), renal acidification (21), and neuron physiology (17), the role of NCOA7 in immunomodulation described here may point to a wide spectrum of actions of NCOA7 isoforms and related proteins. Although our data emphasize a pathobiology in endothelium, the up-regulation of NCOA7 across the pulmonary vascular wall in PAH suggests that pathogenic roles of NCOA7 deficiency are possible in multiple cell types. Recent studies have reported distinct activities of the short-length NCOA7 isoform (16, 17, 20), and our findings emphasize its reliable inducibility. Nonetheless, when considering that the isoforms either singly or together were up-regulated under various disease triggers, our data support the notion of shared and possibly additive or synergistic behavior in lysosomal regulation across both isoforms. This idea is further strengthened by NCOA7 isoforms carrying a Tre2/Bub2/Cdc16 (TBC), lysin motif (LysM), TLDc domain (43). A recent study has demonstrated that all TLDc-containing proteins physically interact with V-ATPases, defining a class of V-ATPase regulatory proteins (18). Our findings indicated that overexpression of full- versus short-length NCOA7 induced a higher level of ATP6V1B2-NCOA7 interactions, suggesting that other protein domains in the full-length isoform could enhance

Fig. 7. Computational modeling identifies 958_{ami} as an NCOA7 activator that abrogates endothelial immunoactivation and PAH. (A to C) Computational protocol for identifying small-molecule modulators of NCOA7, composed of three major components: (A) druggability simulations, (B) pharmacophore modeling, and (C) virtual screening. (D and E) Refinement of the identified compound 958 after molecular dynamics simulations into its analog 958_{ami}. Interactions between compound atoms and NCOA7 residues are shown in two dimensions. Stronger interactions are indicated with orange dashed lines, and weaker interactions are indicated with gray dashed lines. Orange solid lines are strong or persistent interactions with more than 0.3 μs cumulative duration per interaction over 0.6 μs total simulations. (F) Association of the V-ATPase subunit ATP6V1B2 with NCOA7 measured by means of proximity ligation assay (orange). The images demonstrate dual incubation of ATP6V1B2 and NCOA7 antibodies with DMSO or 958_{ami} (20 μM).



(P) CH25H expression by means of RT-qPCR ($n = 3$ replicates per group; two-way ANOVA). (Q) Expression of VCAM1 by means of RT-qPCR and (R) immunoblot in PAECs treated with DMSO versus 958_{ami} ($n = 3$ replicates per group; two-way ANOVA). (N) Rats were administered monocrotaline (80 mg/kg intraperitoneally) 1 week before initiation of a daily dose of 958_{ami} (7.5 mg/kg intraperitoneally) for 10 days. (O) Pulmonary arterioles from DMSO- versus 958_{ami}-injected rats stained for a target protein (CH25H, VCAM1, or CD11b; red with yellow arrowheads), the endothelial layer (CD31; green), the smooth muscle layer (α -SMA; white), and nuclear counterstain (DAPI; blue). (P to S) Quantification of the relative intensity of (P) CH25H or (Q) VCAM1, (R) the number of CD11b⁺ cells per vessel, or (S) the degree of vessel muscularization defined by α -SMA layer thickness to total vessel diameter ($n = 6$ to 7 rats per group). (T) Fulton's Index, (U) RVFAC, (V) TAPSE, and (W) RVSP of monocrotaline rats receiving intraperitoneal DMSO or 958_{ami} ($n = 5$ to 15 rats per group). All data were analyzed by means of Student's *t* test unless otherwise specified and presented as mean \pm SD.

the TLDC domain interaction with V-ATPase subunits. Moreover, a homolog of NCOA7—oxidation resistance protein 1 (OXR1)—has been described as an anti-inflammatory factor (65), presumably through control of lysosomal function (66). Future work should address whether TLDC-containing proteins carry compensatory or synergistic activity with NCOA7 isoforms in pulmonary vascular disease across lysosomal function and inflammatory cascades.

At the cellular level, our work highlights a distinct lysosomal role in EC function and PAH. Prior clinical observations have suggested a relationship between rare, recessive, loss-of-function LSDs and pulmonary vascular diseases. For example, mutations in V-ATPase subunits present with pulmonary arterial stenosis or hypoplasia and RV hypertrophy (15). PAH has been seen in mucolipidosis—a disease driven by dysfunctional lysosomal enzyme processing (12–14). High pulmonary arterial pressures were reported in patients with Gaucher's disease—a condition resulting from deficiency of lysosomal β -glucuronidase and carrying an association to World Symposium on Pulmonary Hypertension (WSPH) Group 5 PH (7, 67). Moreover, Niemann-Pick disease and Fabry disease manifest with severe pulmonary dysfunction (68), which often coexists with WSPH Group 3 PH. Supported by these rare genetic diseases, the association of the homozygous C/C genotype to worsened survival in PAH offers more definitive proof of a link between lysosomal dysfunction and PAH. As guided by the mean C allele frequency (~0.48 to 0.52) of SNP rs11154337 in the global population, approximately a quarter of all PAH patients should harbor the C/C genotype and would be expected to suffer from worsened mortality. It remains to be seen whether worsened PAH may manifest to an even greater extent in monoallelic carriers of known familial PAH mutations or lysosomal enzyme mutations if accompanied by the SNP rs11154337 C/C genotype. Other studies have implicated both BMPR2 and autophagy to lysosomal activity in complex contexts in PAH (24, 27). Yet because neither BMPR2 nor autophagy are predominantly linked to NCOA7 deficiency in the endothelium, there may exist an even broader spectrum of pathogenic lysosomal activities in PAH operating in parallel to NCOA7 deficiencies.

Our work advances the relevance of oxysterol and bile acid metabolism to immunoactivation of the endothelium (33). Elevated oxysterols have been reported in serum and lung tissue in PAH (69–71), and small studies have demonstrated the elevation of bile acids in PAH plasma and lung tissue (29–31, 72). Consistent with our studies of endothelial oxysterol production (35), pulmonary tissue, rather than liver tissue, has been described as a major source of circulating extrahepatic bile acids (73). Given our findings that NCOA7-dependent

proliferative activity is not CH25H-dependent and that individual intermediates across the spectrum of oxysterol metabolism carry both inflammatory activity and association to PAH mortality, future studies should explore any additive pathobiology of the entire complement of oxysterols and bile acids. It is possible that dynamic profiles of these metabolites may display a sex dependence, perhaps relevant to known sex differences in inflammation and the worsened survival rates in men with PAH (74). This includes not only 25HC, which carries pleiotropic roles in innate and adaptive immunity (32) and peripheral vascular disease (75, 76), but also 7HOCA, which has been recently linked to RV improvement with ranolazine treatment in PAH (72). Our findings emphasized the relationship of these metabolites to metrics of disease severity rather than the risk of PAH. As such, in contrast to a single trigger, oxysterol-induced inflammation may act as a “second hit” to worsen PAH, thus aligning with evidence of inflammation and immune dysregulation in this complex disease.

Beyond oxysterols, our study also highlights the potential relevance of upstream, systemic cholesterol metabolism in PAH. Reports of high-density lipoprotein (HDL) and low-density lipoprotein (LDL) elevations in PAH have been inconsistent (77–81). These discrepancies across small studies could be attributed to the complex biology of de novo synthesis, uptake, and cellular processing of cholesterol. Alternatively, a more obvious association of HDL and LDL levels may emerge in PAH populations if segregated by the SNP rs11154337 genotype. Future work will be necessary to better understand both the systemic and cellular kinetics of total cholesterol metabolism in PAH.

From a translational perspective, the integration of population-level genomic and metabolomic data with mechanistic experimentation offers a foundation for the development of prognostic biomarkers in PAH. Although risk calculation has been implemented in clinical practice (82, 83), issues of sensitivity and specificity still plague prognostics, with continued reliance on invasive hemodynamic measurements of disease (84). As discussed by Alotaibi *et al.* (35), assessment of oxysterol and bile acid plasma signatures offers a noninvasive approach to improve risk calculation and guide clinical management. The evaluation of SNP rs11154337 carries potential to improve prognosis and possibly also guide more aggressive, targeted therapy. Given the high C and G allele frequencies of this SNP, such genotyping would be relevant to a large portion of PAH patients. Furthermore, considering the wide effects of NCOA7 on inflammation and EC biology, severity indices of other peripheral vascular diseases may associate with this SNP genotype. For example, the relationship between NCOA7 and severe acute respiratory syndrome coronavirus 2 (SARS-

CoV-2) cellular entry (20), as well as the upregulation of CH25H and oxysterols in COVID-19 (85), suggest that SNP rs11154337 may also predict risk or severity of disease in acute COVID-19 or post-acute sequelae of COVID-19.

Last, our findings provide a roadmap toward next-generation therapies in PAH and conditions of immune dysregulation. Given the link between SNP rs11154337 of NCOA7 and EC inflammation, genotyping patients could foster a precision medicine approach in the recruitment and study of candidates for anti-inflammatory therapies that have had equivocal results when not guided by such rationale (86). Because our findings suggest that SNP rs11154337 depends in part on PVR but also on mechanisms independent of PVR to affect morbidity and mortality, trials that evaluate NCOA7-based and other anti-inflammatory agents should not rely solely on PVR and hemodynamic improvement as surrogate markers indicative of mortality and morbidity benefit. Thus far, our work offers a single example of computational modeling to identify effective small molecules that activate NCOA7. This strategy can now be expanded to develop a portfolio of therapeutic agonists of the NCOA7 TLDC domain or inhibitors of oxysterol and bile acid production to improve existing PAH. Our work was limited by testing 958_{ami} in only a single inflammatory model of PAH, and therefore additional studies of this drug are warranted in other models. Nonetheless, therapies such as 958_{ami} may offer a complement to existing vasodilator therapies or other agents that mainly target cellular proliferative and survival pathways (87). Moreover, beyond PAH, it is possible that NCOA7 therapies could modulate adaptive and innate immunity across other diseases in which NCOA7 is enriched, such as in autoimmune, neurologic, pulmonary, renal, and reproductive contexts.

Through multidimensional analyses of genomic and metabolomic datasets in combination with *in vitro* and *in vivo* mechanistic validation, we defined the fundamental and SNP-dependent role of NCOA7 and its control of lysosomal activity and sterol homeostasis to temper inflammation, EC dysfunction, and PAH. Ultimately, our work links inflammation to lysosomal biology and oxysterol metabolism, with implications for molecular diagnostic and therapeutic development not only in PAH but potentially also in other vascular disorders and diseases of immune dysregulation.

Materials and methods

Animal studies

Animal studies were approved by the Division of Laboratory Animal Resources and the Institutional Review Board at the University of Pittsburgh. Given the known differences in basal and induced inflammation across sexes, pooling of sexes across cohorts was not recommended, and male rats and mice were studied (74). The

mouse line in which *Ncoa7* was deleted [C57BL/6 *Ncoa7tm1.1(KOMP)Vlcg*] was obtained from the Knockout Mouse Project (KOMP; <https://komp.org>) and generated by using sperm for rederivation at the Genome Editing, Transgenic, and Virus Core at Magee Women's Research Institute. Obtained mice were bred in-house to generate homozygous, *Ncoa7*-deleted mice. To elicit a model of pulmonary inflammation resulting in severe PH, *Ncoa7*-deleted mice were cross-bred with C57BL/6 *Il6* transgenic (*Tg⁺*) mice. The *Il6**Tg⁺* mice contain a Clara cell 10-kD promoter (CC10) that drives constitutive expression of IL-6 within the lung (56). Mice were 15 to 16 weeks of age, with the last 4 weeks under chronic hypoxia before echocardiography, invasive hemodynamics measurement, and tissue harvesting. Similarly aged *Il6**Tg⁺* mice were used for an endothelial-specific *Ncoa7*-deactivation experiment by use of polymeric 7C1 nanoparticles composed of low-molecular-weight polyamines and lipids. Small interfering RNA (siRNA) oligonucleotides against negative control or mouse *Ncoa7* (both short and full length isoforms) (siNc and si*Ncoa7*, respectively; Stealth RNAi, ThermoFisher, 12935300 and 1320001, respectively) were encapsulated within the 7C1 nanoparticles for selective delivery to the endothelium, as described (88). Mice received five tail vein injections of 7C1:siNc or 7C1:si*Ncoa7* (1 mg/kg) at 5-day intervals for 25 days. Mice were taken to 15 to 16 weeks of age before echocardiography, invasive hemodynamics measurement, and tissue harvesting. C57BL/6 mice were used for orotracheal delivery of either phosphate-buffered saline (PBS) or 7HOCA (10 mg/kg) serially injected every 5 days for 4 weeks under chronic hypoxia (10% O₂; OxyCycler chamber, BioSpherix). Mice were taken to 15 to 16 weeks of age under normal oxygen tension before echocardiography, invasive hemodynamics measurement, and tissue harvesting. A monocrotaline rat model of PAH was used with a single injection of monocrotaline (80 mg/kg) at 8 to 9 weeks of age. Rats were then injected intraperitoneally with DMSO or 958_{ami} (7.5 mg/kg) for 10 days after monocrotaline loading dose before echocardiography, invasive hemodynamics measurement, and tissue harvesting.

Human subjects

Experimental procedures with human tissue, plasma, or hemodynamics were approved by the institutional review boards of all participating centers. Informed consent was obtained for all recruited human participants. Ethical approval was consistent with the Declaration of Helsinki.

Human cohorts and biobanked samples

The choice to study specific cohorts and samples was driven by availability of patient data and tissue and subsequent statistical calculations of study power.

Biobanked cells and tissue

Parental iPSC line was SNP sequenced from a healthy female control and subsequently SNP-edited to produce the isogenic cell lines (89). PAH lung tissue was harvested from PAH patients at the time of lung transplant and was described previously (22). Histologic assessment of pulmonary arterioles was chosen from an assembled biobank of Group I PAH patient tissue derived at the time of lung transplant or death followed by rapid autopsy (table S2) and described previously (90).

Human PAH cohorts

For plasma metabolite analyses, a single-center PAH cohort was studied from the University of Pittsburgh Medical Center (*n* = 116, in which patients had available plasma samples) (table S1), which we named UPMC-a. For SNP genotype analyses, a single-center PAH discovery cohort was studied of European-descent subjects from the University of Pittsburgh Medical Center (*n* = 93) (Table 1). We named this cohort UPMC-b, a partially overlapping but not fully identical cohort to UPMC-a, given the existing availability of DNA versus plasma samples to analyze. For a validation cohort for SNP genotype analyses, we describe the STRIDE+ cohort (*n* = 630) (Table 1 and table S3), a multicenter PAH cohort of European-descent PAH patients derived both from prospective recruitment and from retrospective inclusion of PAH patients from the Sitaxsentan To Relieve Impaired Exercise (STRIDE) trial (comprising 45 US and Canadian pulmonary hypertension centers).

Statistics

All in vitro data represent at least three independent experiments. The number of animals used for a given experimental model was calculated to measure at least a 20% difference between the means of the control and experimental groups, with a power of 80% and a standard deviation (SD) of 10%. The number of patient samples used for molecular analyses was primarily determined by clinical availability. For normally distributed data, paired data were analyzed with a two-tailed Student's *t* test, and grouped data were compared with either a one- or two-way analysis of variance (ANOVA), with post hoc Tukey analysis to adjust for multiple comparisons. Significance was determined by a *P* value of <0.05. All data are presented as mean ± SD.

Additional information regarding materials and methods can be found in the supplementary materials.

REFERENCES AND NOTES

- M. Bäck, A. Yurdagul Jr., I. Tabas, K. Öörni, P. T. Kovanen, Inflammation and its resolution in atherosclerosis: Mediators and therapeutic opportunities. *Nat. Rev. Cardiol.* **16**, 389–406 (2019). doi: [10.1038/s41569-019-0169-2](https://doi.org/10.1038/s41569-019-0169-2); pmid: [30846875](https://pubmed.ncbi.nlm.nih.gov/30846875/)
- T. J. Guzik, R. M. Touyz, Oxidative stress, inflammation, and vascular aging in hypertension. *Hypertension* **70**, 660–667 (2017). doi: [10.1161/HYPERTENSIONAHA.117.07802](https://doi.org/10.1161/HYPERTENSIONAHA.117.07802); pmid: [28784646](https://pubmed.ncbi.nlm.nih.gov/28784646/)
- P. J. Kelly, R. Lemmens, G. Tsivgoulis, Inflammation and stroke risk: A new target for prevention. *Stroke* **52**, 2697–2706 (2021). doi: [10.1161/STROKEAHA.121.034388](https://doi.org/10.1161/STROKEAHA.121.034388); pmid: [34162215](https://pubmed.ncbi.nlm.nih.gov/34162215/)
- Y. Hattori, K. Hattori, T. Machida, N. Matsuda, Vascular endotheliitis associated with infections: Its pathogenetic role and therapeutic implication. *Biochem. Pharmacol.* **197**, 114909 (2022). doi: [10.1016/j.bcp.2022.114909](https://doi.org/10.1016/j.bcp.2022.114909); pmid: [35021044](https://pubmed.ncbi.nlm.nih.gov/35021044/)
- J. H. Jones, R. D. Minshall, Endothelial transcytosis in acute lung injury: Emerging mechanisms and therapeutic approaches. *Front. Physiol.* **13**, 828093 (2022). doi: [10.3389/fphys.2022.828093](https://doi.org/10.3389/fphys.2022.828093); pmid: [35431977](https://pubmed.ncbi.nlm.nih.gov/35431977/)
- H. M. Otifi, B. K. Adiga, Endothelial dysfunction in COVID-19 infection. *Am. J. Med. Sci.* **363**, 281–287 (2022). doi: [10.1016/j.jams.2021.12.010](https://doi.org/10.1016/j.jams.2021.12.010); pmid: [35093394](https://pubmed.ncbi.nlm.nih.gov/35093394/)
- G. Simonneau et al., Haemodynamic definitions and updated clinical classification of pulmonary hypertension. *Eur. Respir. J.* **53**, 180193 (2019). doi: [10.1183/13993003.01913-2018](https://doi.org/10.1183/13993003.01913-2018); pmid: [30545968](https://pubmed.ncbi.nlm.nih.gov/30545968/)
- W. M. Kuebler et al., A pro-con debate: Current controversies in PAH pathogenesis at the American Thoracic Society International Conference in 2017. *Am. J. Physiol. Lung Cell. Mol. Physiol.* **315**, L502–L516 (2018). doi: [10.1152/ajplung.00150.2018](https://doi.org/10.1152/ajplung.00150.2018); pmid: [29877097](https://pubmed.ncbi.nlm.nih.gov/29877097/)
- C. Nathan, A. Ding, Nonresolving inflammation. *Cell* **140**, 871–882 (2010). doi: [10.1016/j.cell.2010.02.029](https://doi.org/10.1016/j.cell.2010.02.029); pmid: [20303877](https://pubmed.ncbi.nlm.nih.gov/20303877/)
- M. Cao, X. Luo, K. Wu, X. He, Targeting lysosomes in human disease: From basic research to clinical applications. *Signal Transduct. Target. Ther.* **6**, 379 (2021). doi: [10.1038/s41392-021-00778-y](https://doi.org/10.1038/s41392-021-00778-y); pmid: [34744168](https://pubmed.ncbi.nlm.nih.gov/34744168/)
- J. A. Mindell, Lysosomal acidification mechanisms. *Annu. Rev. Physiol.* **74**, 69–86 (2012). doi: [10.1146/annurev-physiol-012110-142317](https://doi.org/10.1146/annurev-physiol-012110-142317); pmid: [22335796](https://pubmed.ncbi.nlm.nih.gov/22335796/)
- M. Alfadhel, W. AlShehhi, H. Alshaalan, M. Al Balwi, W. Eyaid, Mucolipidoses II: First report from Saudi Arabia. *Ann. Saudi Med.* **33**, 382–386 (2013). doi: [10.5144/0256-4947.2013.382](https://doi.org/10.5144/0256-4947.2013.382); pmid: [24060719](https://pubmed.ncbi.nlm.nih.gov/24060719/)
- M. Ishak, E. V. Zambrano, A. Bazzy-Asaad, A. E. Esquibies, Unusual pulmonary findings in mucolipidosis II. *Pediatr. Pulmonol.* **47**, 719–721 (2012). doi: [10.1002/ppul.21599](https://doi.org/10.1002/ppul.21599); pmid: [22162509](https://pubmed.ncbi.nlm.nih.gov/22162509/)
- S. Recla, A. Hahn, C. Apitz, Pulmonary arterial hypertension associated with impaired lysosomal endothelin-1 degradation. *Cardiol. Young* **25**, 773–776 (2015). doi: [10.1017/S1047951114000997](https://doi.org/10.1017/S1047951114000997); pmid: [24910177](https://pubmed.ncbi.nlm.nih.gov/24910177/)
- T. Van Damme et al., Mutations in ATP6V1E1 or ATP6V1A cause autosomal-recessive cutis laxa. *Am. J. Hum. Genet.* **100**, 216–227 (2017). doi: [10.1016/j.ajhg.2016.12.010](https://doi.org/10.1016/j.ajhg.2016.12.010); pmid: [28065471](https://pubmed.ncbi.nlm.nih.gov/28065471/)
- T. Doyle et al., The interferon-inducible isoform of NCOAT inhibits endosome-mediated viral entry. *Nat. Microbiol.* **3**, 1369–1376 (2018). doi: [10.1038/s41564-018-0273-9](https://doi.org/10.1038/s41564-018-0273-9); pmid: [30478388](https://pubmed.ncbi.nlm.nih.gov/30478388/)
- E. Castroflorio et al., The *Ncoa7* locus regulates V-ATPase formation and function, neurodevelopment and behaviour. *Cell. Mol. Life Sci.* **78**, 3503–3524 (2021). doi: [10.1007/s00108-020-03721-6](https://doi.org/10.1007/s00108-020-03721-6); pmid: [33400696](https://pubmed.ncbi.nlm.nih.gov/33400696/)
- A. F. Eaton, D. Brown, M. Merkulova, The evolutionary conserved TLDc domain defines a new class of (H⁺)V-ATPase interacting proteins. *Sci. Rep.* **11**, 22654 (2021). doi: [10.1038/s41598-021-01809-y](https://doi.org/10.1038/s41598-021-01809-y); pmid: [34811399](https://pubmed.ncbi.nlm.nih.gov/34811399/)
- Z. Wang, C. D. Berkey, P. I. Watnick, The *Drosophila* protein mustard tailors the innate immune response activated by the immune deficiency pathway. *J. Immunol.* **188**, 3993–4000 (2012). doi: [10.4049/jimmunol.1103301](https://doi.org/10.4049/jimmunol.1103301); pmid: [22427641](https://pubmed.ncbi.nlm.nih.gov/22427641/)
- H. Khan et al., TMPRSS2 promotes SARS-CoV-2 evasion from NCOAT-mediated restriction. *PLOS Pathog.* **17**, e1009820 (2021). doi: [10.1371/journal.ppat.1009820](https://doi.org/10.1371/journal.ppat.1009820); pmid: [34807954](https://pubmed.ncbi.nlm.nih.gov/34807954/)
- M. Merkulova et al., Targeted deletion of the *Ncoa7* gene results in incomplete distal renal tubular acidosis in mice. *Am. J. Physiol. Renal Physiol.* **315**, F173–F185 (2018). doi: [10.1152/ajprenal.00407.2017](https://doi.org/10.1152/ajprenal.00407.2017); pmid: [29384414](https://pubmed.ncbi.nlm.nih.gov/29384414/)
- V. Negi et al., Computational repurposing of therapeutic small molecules from cancer to pulmonary hypertension. *Sci. Adv.* **7**, eabb3794 (2021). doi: [10.1126/sciadv.eabb3794](https://doi.org/10.1126/sciadv.eabb3794); pmid: [34669463](https://pubmed.ncbi.nlm.nih.gov/34669463/)
- D. Saygin et al., Transcriptional profiling of lung cell populations in idiopathic pulmonary arterial hypertension. *Pulm. Circ.* **10**, 1–15 (2020). doi: [10.1177/2045894020908782](https://doi.org/10.1177/2045894020908782); pmid: [32166015](https://pubmed.ncbi.nlm.nih.gov/32166015/)

24. H. Chichger, S. Rounds, E. O. Harrington, Endosomes and autophagy: Regulators of pulmonary endothelial cell homeostasis in health and disease. *Antioxid. Redox Signal.* **31**, 994–1008 (2019). doi: [10.1089/ars.2019.7817](https://doi.org/10.1089/ars.2019.7817); pmid: [3190562](https://pubmed.ncbi.nlm.nih.gov/3190562/)
25. J. P. Luzio, R. P. Pryor, N. A. Bright, Lysosomes: Fusion and function. *Nat. Rev. Mol. Cell Biol.* **8**, 622–632 (2007). doi: [10.1038/nrm2217](https://doi.org/10.1038/nrm2217); pmid: [17637737](https://pubmed.ncbi.nlm.nih.gov/17637737/)
26. A. C. Racanelli, A. M. K. Choi, M. E. Choi, Autophagy in chronic lung disease. *Prog. Mol. Biol. Transl. Sci.* **172**, 135–156 (2020). doi: [10.1016/bbs.pmbts.2020.02.001](https://doi.org/10.1016/bbs.pmbts.2020.02.001); pmid: [32620240](https://pubmed.ncbi.nlm.nih.gov/32620240/)
27. L. Long et al., Chloroquine prevents progression of experimental pulmonary hypertension via inhibition of autophagy and lysosomal bone morphogenetic protein type II receptor degradation. *Circ. Res.* **112**, 1159–1170 (2013). doi: [10.1161/CIRCRESAHA.111.300483](https://doi.org/10.1161/CIRCRESAHA.111.300483); pmid: [23446737](https://pubmed.ncbi.nlm.nih.gov/23446737/)
28. M. E. G. de Araujo, G. Liebscher, M. W. Hess, L. A. Huber, Lysosomal size matters. *Traffic* **21**, 60–75 (2020). doi: [10.1111/tra.12714](https://doi.org/10.1111/tra.12714); pmid: [31802835](https://pubmed.ncbi.nlm.nih.gov/31802835/)
29. P. Chouvarine et al., Trans-right ventricle and transpulmonary metabolite gradients in human pulmonary arterial hypertension. *Heart* **106**, 1332–1341 (2020). doi: [10.1136/heartjnl-2019-315900](https://doi.org/10.1136/heartjnl-2019-315900); pmid: [32079620](https://pubmed.ncbi.nlm.nih.gov/32079620/)
30. Y. D. Zhao et al., De novo synthesis of bile acids in pulmonary arterial hypertension lung. *Metabolomics* **10**, 1169–1175 (2014). doi: [10.1007/s11306-014-0653-y](https://doi.org/10.1007/s11306-014-0653-y); pmid: [25374487](https://pubmed.ncbi.nlm.nih.gov/25374487/)
31. R. Bujak et al., New biochemical insights into the mechanisms of pulmonary arterial hypertension in humans. *PLOS ONE* **11**, e0160505 (2016). doi: [10.1371/journal.pone.0160505](https://doi.org/10.1371/journal.pone.0160505); pmid: [27486806](https://pubmed.ncbi.nlm.nih.gov/27486806/)
32. J. G. Cyster, E. V. Dang, A. Reboldi, T. Yi, 25-Hydroxycholesterols in innate and adaptive immunity. *Nat. Rev. Immunol.* **14**, 731–743 (2014). doi: [10.1038/nri3755](https://doi.org/10.1038/nri3755); pmid: [25324126](https://pubmed.ncbi.nlm.nih.gov/25324126/)
33. P. Qin, X. Tang, M. M. Ellosi, D. C. Harnish, Bile acids induce adhesion molecule expression in endothelial cells through activation of reactive oxygen species, NF- κ B, and p38. *Am. J. Physiol. Heart Circ. Physiol.* **291**, H741–H747 (2006). doi: [10.1152/ajpheart.01182.2005](https://doi.org/10.1152/ajpheart.01182.2005); pmid: [16582018](https://pubmed.ncbi.nlm.nih.gov/16582018/)
34. Y. Meng, S. Heybrock, D. Nucalai, P. Saftig, Cholesterol handling in lysosomes and beyond. *Trends Cell Biol.* **30**, 452–466 (2020). doi: [10.1016/j.tcb.2020.02.007](https://doi.org/10.1016/j.tcb.2020.02.007); pmid: [32413315](https://pubmed.ncbi.nlm.nih.gov/32413315/)
35. M. Alotaibi et al., Pulmonary primary oxysterol and bile acid synthesis as a predictor of outcomes in pulmonary arterial hypertension. *bioRxiv* 576474 [Preprint] (2024); <https://doi.org/10.1101/2024.01.20.576474>.
36. M. Rabinovitch, C. Guignabert, M. Humbert, M. R. Nicolls, Inflammation and immunity in the pathogenesis of pulmonary arterial hypertension. *Circ. Res.* **115**, 165–175 (2014). doi: [10.1161/CIRCRESAHA.113.301141](https://doi.org/10.1161/CIRCRESAHA.113.301141); pmid: [24951765](https://pubmed.ncbi.nlm.nih.gov/24951765/)
37. W. J. Kent et al., The human genome browser at UCSC. *Genome Res.* **12**, 996–1006 (2002). doi: [10.1101/gr.229102](https://doi.org/10.1101/gr.229102); pmid: [12045153](https://pubmed.ncbi.nlm.nih.gov/12045153/)
38. B. B. Chu et al., Cholesterol transport through lysosome-peroxisome membrane contacts. *Cell* **161**, 291–306 (2015). doi: [10.1016/j.cell.2015.02.019](https://doi.org/10.1016/j.cell.2015.02.019); pmid: [25860611](https://pubmed.ncbi.nlm.nih.gov/25860611/)
39. H. J. Kwon et al., Structure of N-terminal domain of NPC1 reveals distinct subdomains for binding and transfer of cholesterol. *Cell* **137**, 1213–1224 (2009). doi: [10.1016/j.cell.2009.03.049](https://doi.org/10.1016/j.cell.2009.03.049); pmid: [19563754](https://pubmed.ncbi.nlm.nih.gov/19563754/)
40. E. L. Huttlin et al., The BioPlex Network: A systematic exploration of the human interactome. *Cell* **162**, 425–440 (2015). doi: [10.1016/j.cell.2015.06.043](https://doi.org/10.1016/j.cell.2015.06.043); pmid: [26186194](https://pubmed.ncbi.nlm.nih.gov/26186194/)
41. M. Merkulova et al., Mapping the H⁺ (V)-ATPase interactome: Identification of proteins involved in trafficking, folding, assembly and phosphorylation. *Sci. Rep.* **5**, 14827 (2015). doi: [10.1038/srep14827](https://doi.org/10.1038/srep14827); pmid: [26442671](https://pubmed.ncbi.nlm.nih.gov/26442671/)
42. D. E. Johnson, P. Ostrowski, V. Jaumouillé, S. Grinstein, The position of lysosomes within the cell determines their luminal pH. *J. Cell Biol.* **212**, 677–692 (2016). doi: [10.1083/jcb.201507112](https://doi.org/10.1083/jcb.201507112); pmid: [26975849](https://pubmed.ncbi.nlm.nih.gov/26975849/)
43. M. J. Finelli, L. Sanchez-Pulido, K. X. Liu, K. E. Davies, P. L. Oliver, The evolutionarily conserved Tre2/Bub2/Cdc16 (TBC)–lysM motif (LysM), domain catalytic (TLDc) domain is neuroprotective against oxidative stress. *J. Biol. Chem.* **291**, 2751–2763 (2016). doi: [10.1074/jbc.M115.685222](https://doi.org/10.1074/jbc.M115.685222); pmid: [26668325](https://pubmed.ncbi.nlm.nih.gov/26668325/)
44. F. K. Harlan et al., Fluorogenic substrates for visualizing acidic organelle enzyme activities. *PLOS ONE* **11**, e0156312 (2016). doi: [10.1371/journal.pone.0156312](https://doi.org/10.1371/journal.pone.0156312); pmid: [27228111](https://pubmed.ncbi.nlm.nih.gov/27228111/)
45. J. Marciniwz Jr., J. A. Hartsuck, J. Tang, Mode of inhibition of acid proteases by pepstatin. *J. Biol. Chem.* **251**, 7088–7094 (1976). doi: [10.1016/S0021-9258\(17\)32945-9](https://doi.org/10.1016/S0021-9258(17)32945-9); pmid: [993206](https://pubmed.ncbi.nlm.nih.gov/993206/)
46. Z. Diwu, C. S. Chen, C. Zhang, D. H. Klaubert, R. P. Haugland, A novel acidotropic pH indicator and its potential application in labeling acidic organelles of live cells. *Chem. Biol.* **6**, 411–418 (1999). doi: [10.1016/S1074-5521\(99\)80059-3](https://doi.org/10.1016/S1074-5521(99)80059-3); pmid: [10381401](https://pubmed.ncbi.nlm.nih.gov/10381401/)
47. F. M. Platt, B. Boland, A. C. van der Spoel, The cell biology of disease: lysosomal storage disorders: the cellular impact of lysosomal dysfunction. *J. Cell Biol.* **199**, 723–734 (2012). doi: [10.1083/jcb.201208152](https://doi.org/10.1083/jcb.201208152); pmid: [23185029](https://pubmed.ncbi.nlm.nih.gov/23185029/)
48. M. J. Clague, S. Urbé, F. Ariento, J. Gruenberg, Vacuolar ATPase activity is required for endosomal carrier vesicle formation. *J. Biol. Chem.* **269**, 21–24 (1994). doi: [10.1016/S0021-9258\(17\)42302-7](https://doi.org/10.1016/S0021-9258(17)42302-7); pmid: [8276796](https://pubmed.ncbi.nlm.nih.gov/8276796/)
49. R. Kronqvist, P. Leppimäki, P. Mehto, J. P. Slotte, The effect of interleukin 1 beta on the biosynthesis of cholesterol, phosphatidylcholine, and sphingomyelin in fibroblasts, and on their efflux from cells to lipid-free apolipoprotein A-I. *Eur. J. Biochem.* **262**, 939–946 (1999). doi: [10.1046/j.1432-1379.1999.00484.x](https://doi.org/10.1046/j.1432-1379.1999.00484.x); pmid: [10411659](https://pubmed.ncbi.nlm.nih.gov/10411659/)
50. J. Luo, H. Yang, B. L. Song, Mechanisms and regulation of cholesterol homeostasis. *Nat. Rev. Mol. Cell Biol.* **21**, 225–245 (2020). doi: [10.1038/s41580-019-0190-7](https://doi.org/10.1038/s41580-019-0190-7); pmid: [31848472](https://pubmed.ncbi.nlm.nih.gov/31848472/)
51. N. Zelcer, C. Hong, R. Boyadjian, P. Tononoz, LXR regulates cholesterol uptake through Idol-dependent ubiquitination of the LDL receptor. *Science* **325**, 100–104 (2009). doi: [10.1126/science.1168974](https://doi.org/10.1126/science.1168974); pmid: [19520913](https://pubmed.ncbi.nlm.nih.gov/19520913/)
52. A. Beigneux, A. F. Hofmann, S. G. Young, Human CYP7A1 deficiency: Progress and enigmas. *J. Clin. Invest.* **110**, 29–31 (2002). doi: [10.1172/JCI0216076](https://doi.org/10.1172/JCI0216076); pmid: [12093884](https://pubmed.ncbi.nlm.nih.gov/12093884/)
53. F. Luchetti et al., Endothelial cells, endoplasmic reticulum stress and oxysterols. *Redox Biol.* **13**, 581–587 (2017). doi: [10.1016/j.redox.2017.07.014](https://doi.org/10.1016/j.redox.2017.07.014); pmid: [28783588](https://pubmed.ncbi.nlm.nih.gov/28783588/)
54. F. A. Masri et al., Hyperproliferative apoptosis-resistant endothelial cells in idiopathic pulmonary arterial hypertension. *Am. J. Physiol. Lung Cell. Mol. Physiol.* **293**, L548–L554 (2007). doi: [10.1152/ajplung.00428.2006](https://doi.org/10.1152/ajplung.00428.2006); pmid: [17526595](https://pubmed.ncbi.nlm.nih.gov/17526595/)
55. S. Sakao et al., Initial apoptosis is followed by increased proliferation of apoptosis-resistant endothelial cells. *FASEB J.* **19**, 1178–1180 (2005). doi: [10.1096/fj.04-3261fje](https://doi.org/10.1096/fj.04-3261fje); pmid: [15897232](https://pubmed.ncbi.nlm.nih.gov/15897232/)
56. M. K. Steiner et al., Interleukin-6 overexpression induces pulmonary hypertension. *Circ. Res.* **104**, 236–244, 28p, 244 (2009). doi: [10.1161/CIRCRESAHA.108.18204](https://doi.org/10.1161/CIRCRESAHA.108.18204); pmid: [19074475](https://pubmed.ncbi.nlm.nih.gov/19074475/)
57. A. Sydykov et al., Inflammatory mediators drive adverse right ventricular remodeling and dysfunction and serve as potential biomarkers. *Front. Physiol.* **9**, 609 (2018). doi: [10.3389/fphys.2018.00609](https://doi.org/10.3389/fphys.2018.00609); pmid: [2987501](https://pubmed.ncbi.nlm.nih.gov/2987501/)
58. M. K. Culley et al., Frataxin deficiency promotes endothelial senescence in pulmonary hypertension. *J. Clin. Invest.* **131**, e136459 (2021). doi: [10.1172/JCI136459](https://doi.org/10.1172/JCI136459); pmid: [33905372](https://pubmed.ncbi.nlm.nih.gov/33905372/)
59. E. Rojano, P. Seoane, J. A. G. Ranea, J. R. Perkins, Regulatory variants: From detection to predicting impact. *Brief. Bioinform.* **20**, 1639–1654 (2019). doi: [10.1093/bib/bby039](https://doi.org/10.1093/bib/bby039); pmid: [29893792](https://pubmed.ncbi.nlm.nih.gov/29893792/)
60. D. Yang et al., 3DIV: A 3D-genome Interaction Viewer and database. *Nucleic Acids Res.* **46** (D1), D52–D57 (2018). doi: [10.1093/nar/gkx1017](https://doi.org/10.1093/nar/gkx1017); pmid: [29106613](https://pubmed.ncbi.nlm.nih.gov/29106613/)
61. R. L. Benza et al., Endothelin-1 pathway polymorphisms and outcomes in pulmonary arterial hypertension. *Am. J. Respir. Crit. Care Med.* **192**, 1345–1354 (2015). doi: [10.1164/rccm.201501-0196OC](https://doi.org/10.1164/rccm.201501-0196OC); pmid: [26252367](https://pubmed.ncbi.nlm.nih.gov/26252367/)
62. M. Gu, Efficient differentiation of human pluripotent stem cells to endothelial cells. *Curr. Protoc. Hum. Genet.* **98**, e64 (2018). doi: [10.1002/cphg.64](https://doi.org/10.1002/cphg.64); pmid: [29979824](https://pubmed.ncbi.nlm.nih.gov/29979824/)
63. A. Bakan, N. Nevins, A. S. Lakhdawala, I. Bahar, Drugability assessment of allosteric proteins by dynamics simulations in the presence of probe molecules. *J. Chem. Theory Comput.* **8**, 2435–2447 (2012). doi: [10.1021/ct300117j](https://doi.org/10.1021/ct300117j); pmid: [22798729](https://pubmed.ncbi.nlm.nih.gov/22798729/)
64. T. Sterling, J. J. Irwin, ZINC 15—Ligand discovery for everyone. *J. Chem. Inf. Model.* **55**, 2324–2337 (2015). doi: [10.1021/acs.jcim.5b00559](https://doi.org/10.1021/acs.jcim.5b00559); pmid: [26479676](https://pubmed.ncbi.nlm.nih.gov/26479676/)
65. Y. Li et al., Delivering oxidation resistance-1 (OXR1) to mouse kidney by genetic modified mesenchymal stem cells exhibited enhanced protection against nephrotoxic serum induced renal injury and lupus nephritis. *J. Stem Cell Res. Ther.* **4**, 231 (2014). pmid: [25995969](https://pubmed.ncbi.nlm.nih.gov/25995969/)
66. J. Wang et al., Loss of oxidation resistance 1, OXR1, is associated with an autosomal-recessive neurological disease with cerebellar atrophy and lysosomal dysfunction. *Am. J. Hum. Genet.* **105**, 1237–1253 (2019). doi: [10.1016/j.ajhg.2019.11.002](https://doi.org/10.1016/j.ajhg.2019.11.002); pmid: [31785787](https://pubmed.ncbi.nlm.nih.gov/31785787/)
67. D. Elstein et al., Echocardiographic assessment of pulmonary hypertension in Gaucher's disease. *Lancet* **351**, 1544–1546 (1998). doi: [10.1016/S0140-6736\(98\)10194-0](https://doi.org/10.1016/S0140-6736(98)10194-0); pmid: [10326537](https://pubmed.ncbi.nlm.nih.gov/10326537/)
68. R. Borie, B. Crestani, A. Guyard, O. Lidove, Interstitial lung disease in lysosomal storage disorders. *Eur. Respir. Rev.* **30**, 200363 (2021). doi: [10.1183/16000617.0363-2020](https://doi.org/10.1183/16000617.0363-2020); pmid: [33927007](https://pubmed.ncbi.nlm.nih.gov/33927007/)
69. S. Sharma et al., Role of oxidized lipids in pulmonary arterial hypertension. *Pulm. Circ.* **6**, 261–273 (2016). doi: [10.1086/687293](https://doi.org/10.1086/687293); pmid: [27683603](https://pubmed.ncbi.nlm.nih.gov/27683603/)
70. A. Al-Husseini et al., Increased eicosanoid levels in the Sugen/chronic hypoxia model of severe pulmonary hypertension. *PLOS ONE* **10**, e0120157 (2015). doi: [10.1371/journal.pone.0120157](https://doi.org/10.1371/journal.pone.0120157); pmid: [25785937](https://pubmed.ncbi.nlm.nih.gov/25785937/)
71. D. J. Ross et al., Proinflammatory high-density lipoprotein results from oxidized lipid mediators in the pathogenesis of both idiopathic and associated types of pulmonary arterial hypertension. *Pulm. Circ.* **5**, 640–648 (2015). doi: [10.1086/683695](https://doi.org/10.1086/683695); pmid: [26697171](https://pubmed.ncbi.nlm.nih.gov/26697171/)
72. Q. J. Han et al., Effects of ranolazine on right ventricular function, fluid dynamics, and metabolism in patients with precapillary pulmonary hypertension: Insights from a longitudinal, randomized, double-blinded, placebo controlled, multicenter study. *Front. Cardiovasc. Med.* **10**, 1118796 (2023). doi: [10.3389/fcvm.2023.1118796](https://doi.org/10.3389/fcvm.2023.1118796); pmid: [37383703](https://pubmed.ncbi.nlm.nih.gov/37383703/)
73. A. Babiker et al., Elimination of cholesterol as cholestenic acid in human lung by sterol 27-hydroxylase: Evidence that most of this steroid in the circulation is of pulmonary origin. *J. Lipid Res.* **40**, 1417–1425 (1999). doi: [10.1016/S0022-2275\(99\)33383-6](https://doi.org/10.1016/S0022-2275(99)33383-6); pmid: [10428977](https://pubmed.ncbi.nlm.nih.gov/10428977/)
74. I. Martínez de Toda et al., Sex differences in markers of oxidation and inflammation. Implications for ageing. *Mech. Ageing Dev.* **211**, 111797 (2023). doi: [10.1016/j.mad.2023.111797](https://doi.org/10.1016/j.mad.2023.111797); pmid: [36868332](https://pubmed.ncbi.nlm.nih.gov/36868332/)
75. Z. J. Ou et al., 25-Hydroxycholesterol impairs endothelial function and vasodilation by uncoupling and inhibiting endothelial nitric oxide synthase. *Am. J. Physiol. Endocrinol. Metab.* **311**, E781–E790 (2016). doi: [10.1152/ajpendo.00218.2016](https://doi.org/10.1152/ajpendo.00218.2016); pmid: [27600825](https://pubmed.ncbi.nlm.nih.gov/27600825/)
76. F. Wang et al., Interferon regulator factor 1/retinoic inducible gene 1 (IRF1/RIG-I) axis mediates 25-hydroxycholesterol-induced interleukin-8 production in atherosclerosis. *Cardiovasc. Res.* **93**, 190–199 (2012). doi: [10.1093/cvr/cvr260](https://doi.org/10.1093/cvr/cvr260); pmid: [21979142](https://pubmed.ncbi.nlm.nih.gov/21979142/)
77. N. Al-Namani et al., Prognostic significance of biomarkers in pulmonary arterial hypertension. *Ann. Am. Thorac. Soc.* **13**, 25–30 (2016). doi: [10.1513/AnnalsATS.201508-5430C](https://doi.org/10.1513/AnnalsATS.201508-5430C); pmid: [26501464](https://pubmed.ncbi.nlm.nih.gov/26501464/)
78. K. Jonas et al., High-density lipoprotein cholesterol levels and pulmonary artery vasoactivity in patients with idiopathic pulmonary arterial hypertension. *Pol. Arch. Intern. Med.* **128**, 440–446 (2018). doi: [10.5172/pam.20057380](https://doi.org/10.5172/pam.20057380)
79. G. Kopček et al., Low-density lipoprotein cholesterol and survival in pulmonary arterial hypertension. *Sci. Rep.* **7**, 41650 (2017). doi: [10.1038/srep41650](https://doi.org/10.1038/srep41650); pmid: [28198422](https://pubmed.ncbi.nlm.nih.gov/28198422/)
80. C. M. Larsen et al., Usefulness of high-density lipoprotein cholesterol to predict survival in pulmonary arterial hypertension. *Am. J. Cardiol.* **118**, 292–297 (2016). doi: [10.1016/j.amjcard.2016.04.028](https://doi.org/10.1016/j.amjcard.2016.04.028); pmid: [27291969](https://pubmed.ncbi.nlm.nih.gov/27291969/)
81. S. Umar et al., Involvement of low-density lipoprotein receptor in the pathogenesis of pulmonary hypertension. *J. Am. Heart Assoc.* **9**, e012063 (2020). doi: [10.1161/JAHA.119.012063](https://doi.org/10.1161/JAHA.119.012063); pmid: [31914876](https://pubmed.ncbi.nlm.nih.gov/31914876/)
82. M. Humbert et al., Risk assessment in pulmonary arterial hypertension and chronic thromboembolic pulmonary hypertension. *Eur. Respir. J.* **53**, 180204 (2019). doi: [10.1183/13993003.02004-2018](https://doi.org/10.1183/13993003.02004-2018); pmid: [30923187](https://pubmed.ncbi.nlm.nih.gov/30923187/)
83. M. D. McGoon, D. P. Miller, REVEAL: A contemporary US pulmonary arterial hypertension registry. *Eur. Respir. Rev.* **21**, 8–18 (2012). doi: [10.1183/09059180.00008211](https://doi.org/10.1183/09059180.00008211); pmid: [23739169](https://pubmed.ncbi.nlm.nih.gov/23739169/)
84. A. Frost et al., Diagnosis of pulmonary hypertension. *Eur. Respir. J.* **53**, 1801904 (2019). doi: [10.1183/13993003.01904-2018](https://doi.org/10.1183/13993003.01904-2018); pmid: [30549972](https://pubmed.ncbi.nlm.nih.gov/30549972/)
85. C. X. Foo et al., GPR183 antagonism reduces macrophage infiltration in influenza and SARS-CoV-2 infection. *Eur. Respir. J.* **61**, 2201306 (2023). doi: [10.1183/13993003.01306-2022](https://doi.org/10.1183/13993003.01306-2022); pmid: [36396144](https://pubmed.ncbi.nlm.nih.gov/36396144/)
86. R. T. Zamanian et al., Safety and efficacy of B-cell depletion with rituximab for the treatment of systemic sclerosis-associated pulmonary arterial hypertension: A multicenter, double-blind, randomized, placebo-controlled trial. *Am. J. Respir. Crit. Care Med.* **204**, 209–221 (2021). doi: [10.1164/rccm.202009-3481OC](https://doi.org/10.1164/rccm.202009-3481OC); pmid: [33651671](https://pubmed.ncbi.nlm.nih.gov/33651671/)
87. M. M. Hoeper et al., Phase 3 trial of sotatercept for treatment of pulmonary arterial hypertension. *N. Engl. J. Med.* **388**,

- 1478–1490 (2023). doi: [10.1126/science.adn7277](https://doi.org/10.1126/science.adn7277); pmid: [36877098](https://pubmed.ncbi.nlm.nih.gov/36877098/)
88. J. E. Dahlman *et al.*, In vivo endothelial siRNA delivery using polymeric nanoparticles with low molecular weight. *Nat. Nanotechnol.* **9**, 648–655 (2014). doi: [10.1038/nnano.2014.84](https://doi.org/10.1038/nnano.2014.84); pmid: [24813696](https://pubmed.ncbi.nlm.nih.gov/24813696/)
89. H. Wu *et al.*, Modelling diastolic dysfunction in induced pluripotent stem cell-derived cardiomyocytes from hypertrophic cardiomyopathy patients. *Eur. Heart J.* **40**, 3685–3695 (2019). doi: [10.1093/euroheartj/ehz326](https://doi.org/10.1093/euroheartj/ehz326); pmid: [31219556](https://pubmed.ncbi.nlm.nih.gov/31219556/)
90. T. Bertero *et al.*, Vascular stiffness mechanoactivates YAP/TAZ-dependent glutaminolysis to drive pulmonary hypertension. *J. Clin. Invest.* **126**, 3313–3335 (2016). doi: [10.1172/JCI86387](https://doi.org/10.1172/JCI86387); pmid: [27548520](https://pubmed.ncbi.nlm.nih.gov/27548520/)

ACKNOWLEDGMENTS

We thank the University of Pittsburgh HSCRF Genomics Research Core (RRID: SCR_018301; D. Hollingshead, W. Horne, and J. Lamb) for transcriptomic analyses. We thank the STRIDE consortium for access to their genomic data. We thank the Unified Flow Core at the University of Pittsburgh for use of their instruments. We thank the University of Pittsburgh Small Animal Ultrasonography Core. We thank the Center for Biologic Imaging at the University of Pittsburgh for technical assistance and use of their facilities. We thank the Center for Organ Recovery and Education, the organ donors, and their families for the tissue samples provided for this work. We thank the Pharmacogenomics Research Network–Riken Center for Genomic Medicine Collaborative Studies: RIKEN VI for sharing of patient data. We thank J. Yang, R. Saggar, W. D. Wallace, D. J. Ross, A. Handen, M. Mitsche, and R. Farese for aid in providing study samples and their expert consultations. **Funding:** This work was supported by National Institutes of Health grants F30 HL143879 (L.D.H.); K08 HL166950 (M.A.); R01 HL124021, HL122596, HL151228, and P50 AR080612 (S.Y.C.); R01 HL478946 and R01 HL078946 (R.L.B.); R24 HL105333 and R01 HL160941 (W.C.N.); R01 HL160941 (A.A.D.); R01 GM139297 (I.B.); 1S10 OD025041 (C.M.S.C.; Center for

Biologic Imaging at the University of Pittsburgh); 1S10 OD023684 (University of Pittsburgh Small Animal Ultrasonography Core); T32 HL129964 (N.J.K.); UL1TR003163, 1P30 DK127984, and P01 HL160487 (J.G.M.); WoodNext Foundation (S.Y.C. and I.B.); American Heart Association Established Investigator Award 18EIA33900027 (S.Y.C.); French National Research Agency ANR-18-CE14-0025, ANR-21-CE44-0036, and ANR-20-CE14-0006 (T.B.); French National Cancer Institute INCA-PLBIO 21-094 (T.B.); and US Department of Defense HT9425-24-1-0209 (A.A.D.). **Author contributions:** Conceptualization: L.D.H. and S.Y.C. Methodology: L.D.H., S.Y.C., Y.-Y.T., Y.T., W.E.K., J.Z., C.M.S.C., D.B.S., J.Y.L., M.H.C., S.D., E.G., R.S.M., R.S., K.J.H., A.B.W., S.O., T.-H.S.-A., M.W.P., B.W., A.W., D.G.A., W.C.N., A.A.D., R.L., S.M.N., H.W., J.G.M., I.B., R.L.B., and M.J. Investigation: L.D.H., S.Y.C., M.A., Y.-Y.T., Y.T., H.-J.J.K., N.J.K., W.S., C.-S.C.W., S.A., M.K.C., W.E.K., R.X., Y.A.A., N.H., R.J.R., S.J., V.N., A.K., D.P., A.M.W., C.M.S.C., D.B.S., J.Y.L., M.H.C., M.Z., S.O., B.W., A.W., C.C., S.M.N., J.G.M., and T.B. Visualization: L.D.H. and S.Y.C. Funding acquisition: L.D.H. and S.Y.C. Project administration: L.D.H. and S.Y.C. Supervision: L.D.H. and S.Y.C. Writing – original draft: L.D.H. and S.Y.C. Writing – review and editing: L.D.H., S.Y.C., and S.C. **Competing interests:** S.Y.C. has served as a consultant for Merck, Janssen, and United Therapeutics. S.Y.C. is a director, officer, and shareholder in Synhale Therapeutics. S.Y.C. has held grants from Bayer and United Therapeutics. S.Y.C. and T.B. have filed patent applications regarding metabolism and next-generation therapeutics in pulmonary hypertension (US 10,925,869 B2, “Compositions and methods for treating pulmonary vascular disease”; PCT/US2015/029286, “Coordinate control of pathogenic signaling by the MIR-130-301 family in pulmonary hypertension and fibroproliferative diseases”; PCT/US2018/062013, “Compositions and methods for administering a YAP1/WWRT1 inhibiting composition and a GLS1 inhibiting composition”). S.Y.C., L.D.H., and I.B. have filed patent applications regarding the therapeutic targeting of NCOA7 (US 11,773,391 B2, “Therapeutic and diagnostic target for SARS-CoV-2 and COVID-19”; PCT/IB2023/055431, “Methods and compositions for treatment of

inflammation and inflammatory conditions”). The other authors declare that they have no competing interests. M.J. is an employee of and holds equity in Sapient Bioanalytics for work unrelated to the current manuscript. **Data and materials availability:** All materials used in this study are available to researchers upon reasonable request and after issuance of relevant institutional data sharing agreements by contacting the corresponding author. Human data with identifiers are restricted owing to patient confidentiality. Microarray data have been submitted to Gene Expression Omnibus (GSE250522). All other data and code are included directly in this manuscript or described previously in the respective citations. Human plasma samples and deidentified clinical information were made available from Cincinnati Children’s Hospital Medical Center; plasma metabolomic data were made available from the University of California, San Diego; the *Ncoa7*^{-/-} mouse line was made available from KOMP at the University of California, Davis; and iPSC lines were made available from Stanford University—all under materials transfer agreements with the University of Pittsburgh. **License information:** Copyright © 2025 the authors, some rights reserved; exclusive licensee American Association for the Advancement of Science. No claim to original US government works. <https://www.science.org/about/science-licenses-journal-article-reuse>

SUPPLEMENTARY MATERIALS

science.org/doi/10.1126/science.adn7277

Materials and Methods

Supplementary Text

Figs. S1 to S10

Tables S1 to S11

References (91–142)

MDAR Reproducibility Checklist

Movies S1 to S22

Submitted 8 January 2024; accepted 21 November 2024
10.1126/science.adn7277